Universitetet i Stavanger

FACULTY OF SCIENCE AND TECHNOLOGY

MASTER'S THESIS

Study programme/specialisation: Marine and Offshore Technology	Spring semester, 2021. Open/~~Confidential~~
Author: Priscila Esteves Lopes	…………………………………. (signature of author)
Programme coordinator: Supervisor(s): Dr. Charlotte Obhrai	
Title of master's thesis: Improved Wind Power Estimation Method for Operation & Maintenance of Offshore Wind Farm	
Credits (ECTS): 30	
Keywords: Wind Farm, Offshore, Power Production, Operations & Maintenance, Rotor Equivalent Wind Speed, Hub Height Wind Speed, Power Law, Logarithmic Law	Number of page: 81 + supplemental material/other: Stavanger, 10/07/2021

Abstract

Offshore wind is a rapidly maturing renewable energy technology that is poised to play an important role in future energy systems. In 2018, offshore wind provided a tiny fraction of global electricity supply, but it is set to expand strongly in the coming decades into a USD 1 trillion business (IEA`s 'Renewable Energy Market 2019' report). Turbines are growing in size and in terms of the power capacity they can provide, which in turn is delivering major performance and cost improvements for offshore wind farms.

According to IEC 61400-12-1 standard procedure, for a power curve validation of wind turbines, ideally the measurement of the wind speed would take place at hub height. The underlying assumption is that this measured hub height wind speed sufficiently represents the wind speed across the entire swept area of the turbine rotor. Now that wind turbines are getting bigger, it is very questionable whether the hub height wind speed (HHWS) method is appropriate since it could under-estimate the kinetic energy flux through the rotor area. This can result in inconsistent and potentially incorrect power predictions, which feed into various technical and economic analyses, ranging from grid integration (Mahoney et al., 2012), life-cycle cost analyses (Jong et al., 2017), and capacity expansion studies (Hasager et al., 2015).

This study shows a different method, rotor equivalent wind speed (REWS), in which the wind velocities are measured at several heights across the rotor area and make a comparison of the estimate available power from the HHWS versus REWS methods. Wind speeds extrapolation was made to cover a tip height of 208m, for a 10-MW reference wind turbine, since no wind speed data above 100 m was available for the three different sites, FINO 1, FINO 3 and Frøya.

In order to extrapolate wind speeds at elevations above 100 m up to tip height at 208 m, the power law and the standard logarithmic law wind profiles were assessed to identify a suitable model that could represent offshore wind profile. For the power law, a wind shear coefficient (alpha) was obtained by fitting to the measurements of observed heights. For the logarithmic model, terrain roughness of 0.003 was considered. The result indicates that the power law has better performance with regards to extrapolating wind characteristics for all three different locations.

Finally, the difference between HHWS and REWS available power estimates of ~4.9%, ~3%, and ~8.5% for FINO 1, FINO 3, and Frøya, respectively, illustrate the importance of accounting for rotor-layer wind shear when predicting available power. A comparison to actual power outputs will be a subject of future work. All sites, FINO 1, FINO 3 and Frøya, contain a meteorological mast (MetMast) with a total of 14, 9 and 6 years of weather data, respectively.

KEYWORDS: Wind Farm, Offshore, Power Production, Operations & Maintenance, Rotor Equivalent Wind Speed, Hub Height Wind Speed, Power Law, Logarithmic Law

Acknowledgement

I would like to thank God for one more achievement in my life. Besides, express my gratitude to my supervisor, Dr. Charlotte Obhrai for her support and guidance throughout the course of this thesis work.

In additional, I would like to thank my lover, partner, best friend Alex Greten for all his patience, full support towards our little one during this period and let my dream come true.

Last but not least, I would like to extend my gratitude to all my friends, in and outside school that somehow made this happen, the ones that laugh together, shared jokes but also studied, in special my gratitude to Adham Medhat for his guidance in elaborating this paper and managing Matlab software.

Symbols

Abbreviations

ABL	Atmospheric Boundary Layer
AEP	Annual Energy Production
FEED	Front-end engineering design
HAWT	Horizontal Axis Wind Turbine
HHWS	Hub Height Wind Speed
IEA	International Energy Agency
IEC	International Electrotechnical Committee
KW	Kilowatts
LCoE	Levelized Cost of Energy
MW	Megawatts
O&M	Operation & Maintenance
OSW	Offshore Wind
OWF	Offshore Wind Farm
OWT	Offshore Wind Turbine
REWS	Rotor Equivalent Wind Speed
RMSE	Root Mean Square Error
RSD	Remote Sensing Device
VWP	Vertical Wind Profile
WT	Wind Turbine

List of Figures

List of Tables

1 Introduction

1.1. Motivation and Background

Energy dominated every one of those decades. Consider energy use, say, starting after World War II, from 1950 to 1975. There was power for everything, from seemingly endless sources of oil, gas and coal, and nuclear power was standing by. Next, recall energy from 1975 to 2000. Not so happy. Most shocking – actual energy shortages, and skyrocketing costs. Just as shocking: social and environmental disasters that could no longer be pushed aside, from Exxon Valdez to ruinous strip mines to Three Mile Island to urban smog.

Now, think of the last 19 years. The Bakken Field. The Permian Basin. Deep-water ocean extraction. And a sophisticated industry ready for any play anywhere, operating at peak scientific and technical prowess.

But there were huge changes in the last 19 years. Oil and gas and coal are no longer the whole story. Renewables – solar and wind – have moved closer to center stage, where they will stay, and increase. Why? Because people like renewables. They don't want to feel energy guilt. Or more pointedly, guilty about the impacts of energy, from coal sludge to Deepwater Horizon to the climate to monitoring spent nuclear fuel for a thousand years.

Make no mistake, in the next 80 years the world is fortunate that it will have plentiful quantities of oil and gas – responsibly recovered and produced but in the future sipped, not guzzled, in highly efficient engines.

In the next 80 years the world is doubly fortunate that it has the chance to mainstream electricity generation from renewables, again, primarily wind and solar. These aren't random, disconnected opportunities. Like all progress, these choices are evolutionary, enabled by decisions made, and work started, years ago.

Renewable energy capacity is set to grow 50% between 2019 and 2024, led by solar energy. Solar, wind and hydropower projects are developing at their fastest rate in four years (IEA`s 'Renewable Energy Market 2019' report). In 2020, despite pandemic-induced supply chain challenges and construction delays, renewable capacity additions expanded by more than 45% from 2019 and broke another record (from 190 GW in 2019 to ~280GW in 2020). An exceptional 90% rise in global wind capacity additions led the expansion. Also underpinning this record growth was the 23% expansion of new solar PV (Photovoltaic system) installations to almost 135 GW in 2020 (IEA`s 'Renewable Energy Market Update for 2021 & 2022' report).

Despite declining electricity demand and wholesale power price drops due to the impacts of pandemic, governments around the world auctioned a record amount of renewable energy capacity, awarding almost 75 GW of onshore wind, offshore wind, solar PV and bioenergy in 2020– 20% more than in 2019 (IEA`s 'Renewable Energy Market Update for 2021 & 2022' report).

Countries all over the world are reducing fossil fuel consumption and escalating investments in renewables to provide highest environmental benefit. More than ever, there is a global demand in continuing with implementation of renewable energy methods (solar, wind/wave power, geothermal) to stop global warming in order to achieve Paris Agreement goals.

Ireland, Sweden, Costa Rica, Nicaragua, UK, Germany, Morocco, Kenya, China, USA are leading the way in the switch to renewable energy. Uruguai, for example, it now boasts a national energy supply that's 95% renewables-powered, achieved in less than 10 years. Another one is Denmark, already set a world record in 2014, producing almost 40% of their overall electricity needs from wind power and obtaining 50% of their electricity from renewables in 2019. In Norway, where hydropower is the predominant renewable resource, we can see an increase on development of wind power projects (on and offshore).

Globally, onshore wind capacity is expected to expand by 57% to 850 GW by 2024. United States and China will lead the annual onshore wind additions, owing to a development rush and a policy transition to competitive auctions respectively. Growth will accelerate in the European Union (EU) as competitive auctions continue to maintain costs relatively low. These auctions will mean that expansion in Latin America, the MENA region, Eurasia and sub-Saharan Africa will be stable over the forecast period (*IEA`s 'Renewable 2019' report*).

Offshore wind capacity is forecast to increase almost threefold to 65 GW by 2024, representing almost 10% of total world wind generation. While the EU accounts for half of global OSW capacity expansion over the forecast period, on a country basis, China leads deployment, with 12.5 GW in development. The first large US capacity additions are also expected during the forecast period (*IEA`s 'Renewable 2019' report*).

Wind capacity additions reached almost 114 GW in 2020, almost doubling 2019 expansion. China alone accounted for two-thirds of global wind growth, with Chinese manufacturers supplying turbines for most of the country's installations. At 80 GW, the 2021 wind market is expected to be 30% weaker than last year's, although still significantly exceeding 2019 additions. It is expected slightly lower onshore and offshore growth in 2022. Having reached a record 10% in 2019, the offshore share of total wind additions declined in 2020 but is forecast to rebound to a record-breaking 12% in 2021-2022 (IEA`s 'Renewable Energy Market Update for 2021 & 2022' report).

Moving offshore means high energy potential associated with the vast offshore areas – winds are typically stronger and more stable at sea, resulting in significantly higher production per unit installed. Besides, no limitation for large-scale projects where problems, such as visual impact, noise production and shadow casting won`t affect residents.

Power estimation is based on HHWS concept but with the increase in rotor swept area and hub heights, the impact of wind shear and turbulence intensity become increasingly relevant, and one point measurement from meteorological towers may no longer be good representation of the wind interacting with the turbine (e.g. Sumner et al., 2006, Wagner et al., 2009 and Wharton and Lundquist, 2012). To better improve forecast of power production, this

paper will cover the REWS method, a measure of actual momentum encountered by the turbine by accounting for shear across the rotor disk.

1.2. Wind Turbine Overview

A wind turbine, or wind energy converter, is a device that converts the wind's kinetic energy into electrical energy. It can vary widely in size, with either horizontal or vertical axes.

The length of the blades is the biggest contributor in determining the amount of electricity a WT can generate. Small wind turbines that can power a single home may have an electricity generating capacity of 10 kW. The largest OWT in operation, Haliade X – the prototype in Rotterdam with long blades of 107 meters and 220 meters rotor - operating since late 2019 - has electricity generating capacity of 13 megawatts and larger turbines, up to 15 MW, are in development. Large turbines are often grouped together to create wind power plants, or wind farms, that provides power to electricity grids.

- Horizontal-axis turbines

Horizontal-axis turbines commonly include three blades similar to airplane propellers. Taller turbines with longer blades generate more electricity. Basically, all wind turbines currently in use are horizontal-axis turbines and those will be the object matter of this paper. *Figure 1*

- Vertical-axis turbines

Vertical-axis turbines have blades that are connected to the top and the bottom of a vertical rotor. The most common type of vertical-axis turbine is the Darrieus wind turbine, named after the French engineer Georges Darrieus, who patented the design in 1931. Vertical-axis wind turbines are not much in use today because they do not perform as good as horizontal-axis turbines. *Figure 2*

Figure 1   Horizontal-axis turbine. Source: Adapted from National Energy Education Development Project (public domain)
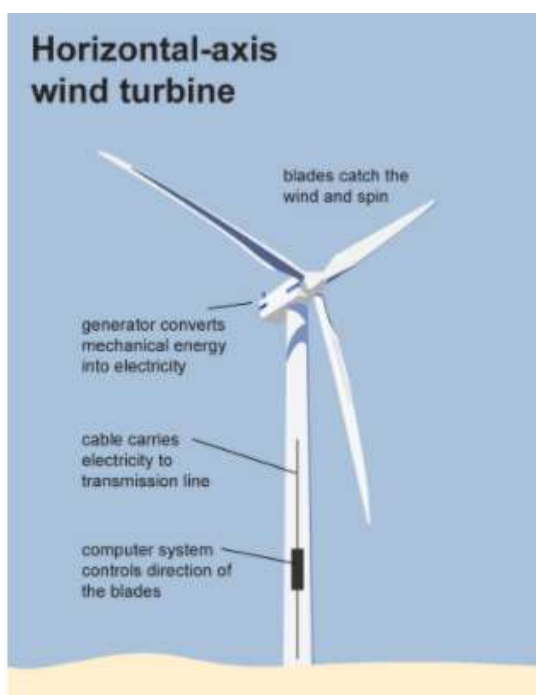
Figure 2 Darrieus vertical-axis wind turbine in Martigny, Switzerland. Source: Lysippos, Wikimedia Commons author (GNU free documentation license) (public domain)

1.2.1 Physical Features of Horizontal Axis Wind Turbine

Some of the main parts composed by a horizontal axis wind turbine, *Figure 3*, are listed below:

The Rotor and Blades

The rotor of a HAWT includes three long blades connected to a horizontal shaft. The blades of the rotor have an aerodynamic shape like airplane wings, so that the uplifting force of the wind can be picked up. A driving torque is then generated by the uplift force causing rotation. When receiving wind, the blades rotate similar to a fan.

The Nacelle

The nacelle that is connected to the rotor houses the operational components such as gearbox, generator, brake, and the controller, supporting the electricity generator of a WT.

The Gearbox

Usually, the rotor rotates at a lower speed. The gearbox turns the slow rotation of the blades into a faster rotation that is more suitable to drive an electrical generator. While the rotor turns at a 20-rpm speed, the generator requires 1000 rpm to generate electricity, on average. The gearbox is located between the rotor and the generator.

The Tower

The rotor and nacelle of a HAWT are placed on top of a tower to capture higher wind speed and avoid turbulent layers of air close to the ground.

The Yaw System

The yaw system drives the turbines towards the wind, making sure that the wind turbine always faces the incoming wind, which is necessary for the rotor blades to pick up wind and start rotating. It is connected with the nacelle, located on top of the tower.
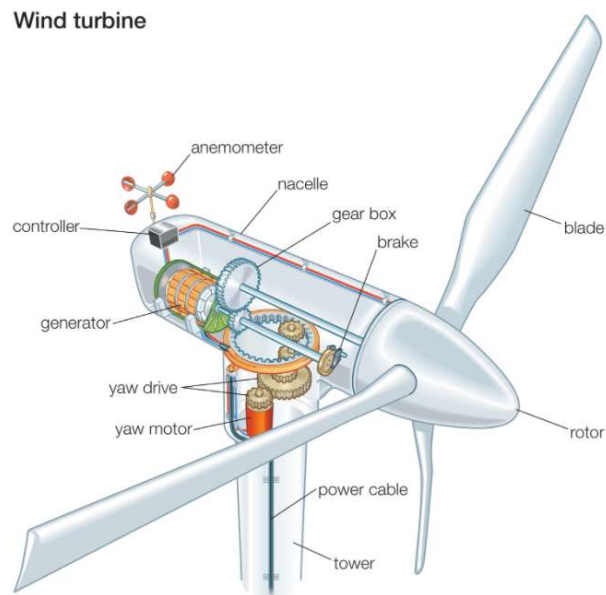
Figure 3 Components of HAWT (public domain)

1.3. Research Project

A service company estimates the power production for operation and maintenance planning of an OWF using the HHWS method, which measures the wind speed at single point (hub height), as recommended by the IEC standard procedure. Nowadays with rotors of modern multi-megawatt wind turbines, this method can be too simplistic to capture accurately the kinetic energy flux through the rotor area resulting in the under-estimation of the power curve validation.

The objective here is to estimate the power production of a 10-MW WTG using wind data from three different locations, FINO 1, FINO 3 and Frøya with a total of 14, 9- and 6-years data, respectively. Two different concepts, HHWS & REWS, will be analyzed and the results will be compared to determine a better approach with regards to power prediction for O&M planning of Offshore Wind Farm.

2. Offshore Wind Farm Overview

2.1 Offshore Wind Farm History

An offshore windfarm contains several horizontal wind turbines located in the same area, producing electricity by harnessing wind energy. In a large wind farm, many turbines can be grouped together. Each turbine consists of the structural parts, foundation and tower, the turbine, and the blades. The turbines are connected to electrical equipment and infrastructure for transmission of electricity to the grid, and control and data acquisition. (Thomsen, 2014).

Offshore wind is a novel (not counting wind power for ships and boats). The first commercial OWF, totaled 5MW, was built in 1991, Vindeby in Denmark.

After the commissioning of Vindeby in 1991, the growth in new OWF was slow. Over the following ten years, only a few more offshore wind farms – in Denmark, Sweden, the Netherlands and the UK – were constructed, the largest being 40MW. Since the farms were considered pilot projects, the political focus was on technical feasibility rather than on comparing costs to other sources of renewable energy.

The first offshore wind farms were relatively simple; onshore turbines based on concrete foundations in shallow water. They were typically ordered by governments and constructed by utilities, sometimes with companies entering into consortia.

While not at industrial scale by any standards, the first offshore wind farms provided valuable learnings. Fundamentally, the projects proved the feasibility of the concept of offshore wind power, despite being harder to install and access. Some early wind farms had positive surprises by producing more energy than expected. This, along with growing political concern over climate change, resulted in an appetite for more offshore wind energy. At the end of 2015, 3.230 turbines at 84 OWFs across 11 European countries had been installed and grid-connected, making for a total capacity of 11.027 MW.

With 6.1 GW of new capacity added, 2019 was the best year in history for the global offshore wind industry, bringing total global cumulative installations to 29.1 GW. China remains in the number one spot for the second year in a row for new installations, installing a record 2.4 GW, followed by the UK at 1.8 GW and Germany at 1.1 GW (*gwec.net – OW report 2020*).

2.1.1 Key Stakeholders of Offshore Wind Farm

In the offshore wind industry, there are three major stakeholders that have the responsibility of the overall windfarm. The three groups are: wind turbine manufactures, wind farm owners, and the offshore transmission owners *Figure 4*. The wind turbine manufactures are always involved in turbine maintenance to some extent at least the first years of operation (Hassan, 2013).
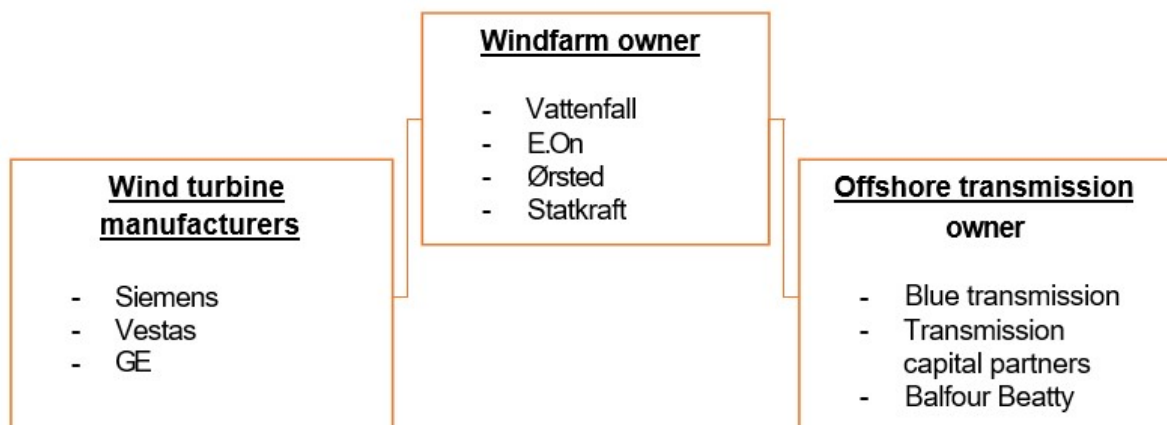
Figure 4 Example of key stakeholders' groups and actors in offshore wind (Hassan, 2013).

2.1.2 Operational System of Horizontal Axis Wind Turbine

Rotor-nacelle assembly, the tower, the transition piece and the support structure make part of a HAWT *Figure 5*. The blades which are comprised by the rotor capture the wind mechanical energy, and the hub, which transmits it to the drive train. Located in the nacelle, the drive train is composed of gearboxes, the generator group, and the power converter, and converts the mechanical energy to electrical energy. As an optional system, depending on the drive train configuration, it is possible to have gearbox and/or power converter. The generated power is transmitted down the turbine tower. As the name indicates, the support structure fixates the turbine on the seabed through different foundation technologies (i.e monopile, gravity-based, tripod, jacket, floating) and is usually connected to the tower by a transition piece. Other terminologies than the one used here can be found, such as in *DNV standard*.

The newest wind turbines are technologically advanced and include engineering and mechanical innovations (i.e. pitch) to help maximize efficiency and increase the production of electricity. WTs structure integrity is monitored by a control system 24/7.

Blade pitch control, *Figure 6*, is a feature of nearly all large modern HAWT. While operating, a wind turbine's control system adjusts the blade pitch to keep the rotor speed within operating limits as the wind speed changes. Feathering the blades stops the rotor during emergency shutdowns, or whenever the wind speed exceeds the maximum rated speed. During construction and maintenance of wind turbines, the blades are usually feathered to reduce unwanted rotational torque in the event of wind gusts.
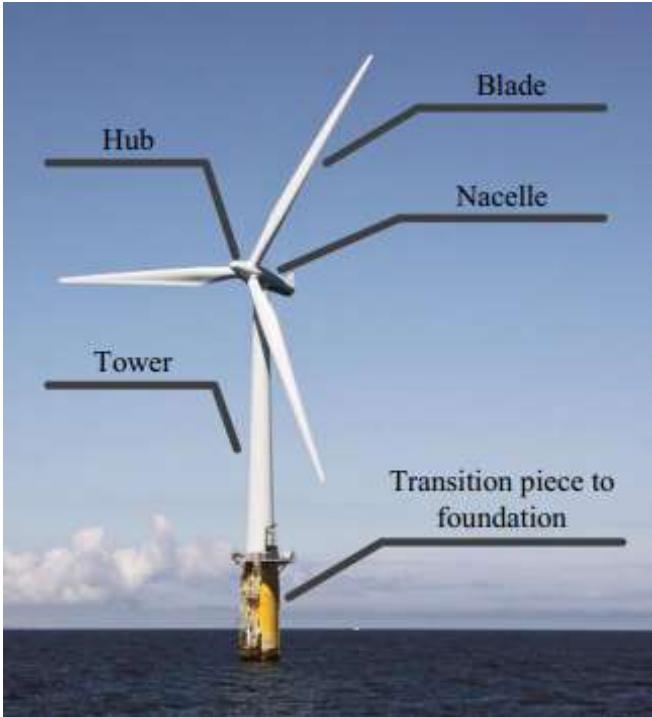
Figure 5 An offshore wind turbine (public domain)
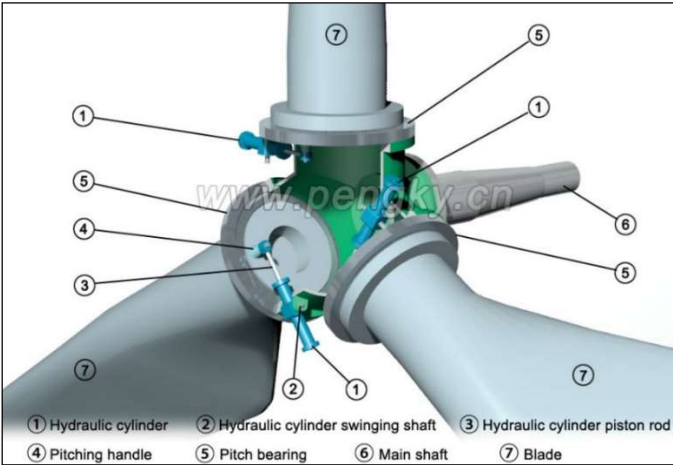
Figure 6 Pitch Control

2.1.3 Lifecycle Processes of Offshore Wind Farm

The offshore wind farm lifecycle is divided into 5 different phases, as illustrated in the picture below. More details of the phases will be covered in the following sections.
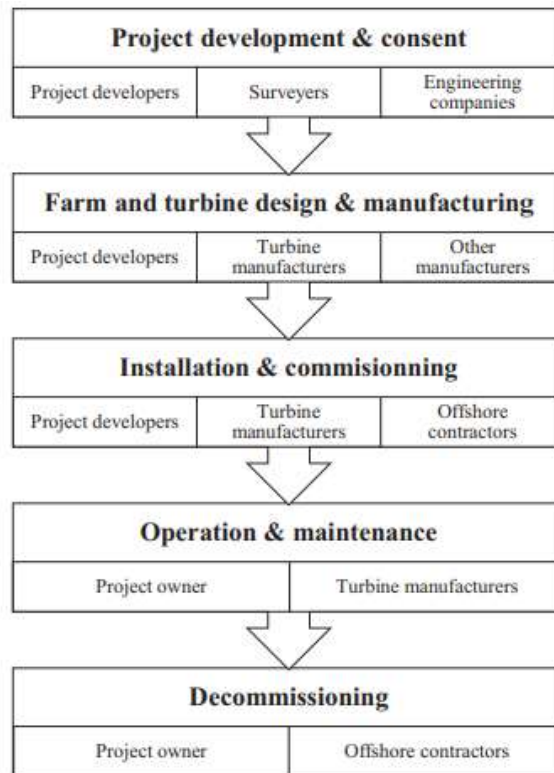
Figure 7 Lifecycle processes of an OWF. (João Dedecca et al., 2016)

2.1.3.1 Project Development & Consent

It consists of surveys on the environment, metrological conditions, seabed conditions, in addition to development surveys (feasibility, licensing, etc.) and FEED studies.

2.1.3.2 Farm and Turbine Design & Manufacturing

It covers the design and manufacturing of the wind turbine by wind turbine manufacturers. Nonetheless, they can act further in the life cycle of the farm, and may install, operate and maintain the wind farm.

2.1.3.3 Installation & Commissioning

It involves the installation and commissioning of the turbine. (Thomsen, 2014). The installation process is when the vessel with the turbine foundations arrives at the wind farm site to install the first foundation and finishes when the cable installation vessels connect all turbines of a wind farm to an offshore substation (Lumbreras et al., 2013 and Yaramasu et al.,

2015). The transmission system then links the offshore substation to the onshore substation through export cables. A wind farm layout can be seen below. *Figure 8*

The commissioning stage covers all activities after all components of the wind turbine are installed. Commissioning tests will generally involve standard electrical tests for the electrical infrastructure as well as the turbine, and inspection of routine civil engineering quality records. It is important to have a careful testing at this stage if a good quality wind farm is to be delivered and maintained.
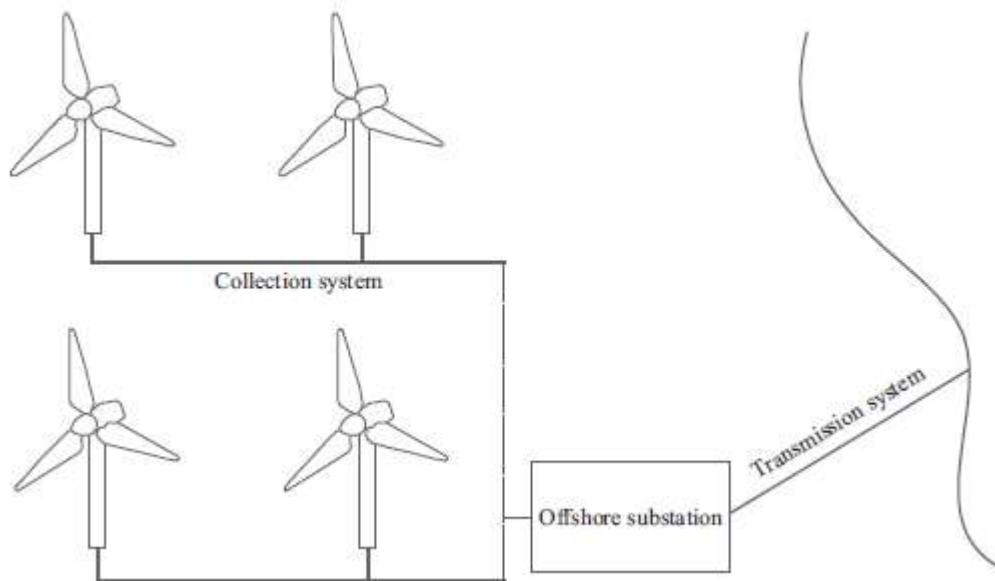
Figure 8 Conceptual offshore wind farm.

The installation of offshore wind farms can be divided in four steps:

1. Foundation installation
2. Turbine installation
   a. Tower
   b. Nacelle
   c. Rotor
   d. Blade
3. Substation installation
   a. Offshore substation
   b. Onshore substation
4. Cable installation
   a. Array cables
   b. Export cables

A brief description of these stages is given below:

Foundation installation

The installation vessel and strategy may differ depending on the foundation type. Nowadays, approximately 90% of OWTs are installed on monopiles and the remainder are installed on jackets, tripods or gravity-based support structures. In addition, there are few demonstration floating turbines, which have no bottom-fixed structure (Asgarpour 2016). A short description of different foundations installation as well as advantages and disadvantages of its structures will be given below.

Monopile Foundations

Monopiles are large hollow steel or concrete tubes *Figure 9*, whose thickness and diameter vary with turbine size, soil conditions and water depth. Before installation of a monopile, a layer of scour protection should be applied to avoid seabed erosion around the monopile. This first scour protection layer is made by rock dumping around the monopile position. When the first layer of scour protection is made, monopiles are lifted from the installation vessel and then positioned on the seabed. They are a common choice for offshore turbines located in shallow water up to 40 m.

Advantages

- → Work well in sand and gravel soils.
- → Have a simple design that installs quickly.
- → Adaptable for shallow and deeper installations of various sizes.
- → Cost-effective for installations to 40 m.

Disadvantages

- → Cost and risks associated with fabrication, installation, and transport increase for larger monopiles required at deeper installations where hydrodynamic loads are an issue.
- → Installation noise can disorient, injure, or kill marine life sensitive to pressure waves. This includes humpback whales, loggerhead turtles and manatees.
- → Wind, wave and seismic loading can negatively affect monopile foundations. This can cause early fatigue damage to the structure if it is not accounted for during installation.
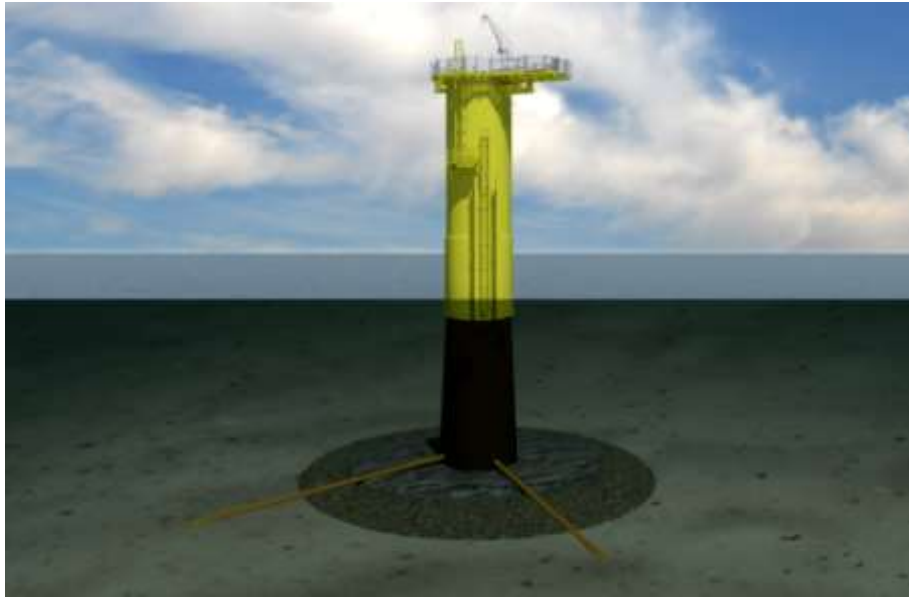
Figure 9 *Monopile foundation (public domain).*

Jacket and Tripod Foundations

Like the monopile installation, a first layer of scour protection by rock dumping is required. The jackets or tripods are transported to the location of the wind farm using jack-up barges or floating vessels with mooring line stabilization. When the installation vessel is positioned, the jacket or tripod is lifted and placed on the seabed. Alternatively, the jacket or tripod can be floated and then, using a crane, be positioned. In that case, a heavy lift crane is no longer required. When the structure is positioned into the location, for jackets, four piles and for tripods, three piles are driven into the seabed to fix the foundation. The pile-driving methods for jackets and tripods are similar to monopiles. When the foundation installation is finished, the turbine tower can be installed directly on the top side of the jacket or the tripod.

Jacket foundations can be installed to depths of 60 m. These lattice-truss structures *Figure 10* bear a resemblance to offshore oil platforms with four tubular legs connected by diagonal struts.

Advantages

- → Can be installed using piles or suction caissons in stiff clays or medium-to-dense sands. Soft-soil installations are possible with longer pile lengths that significantly increase friction resistance.
- → The larger surface area of the lattice configuration may provide an artificial reef location, providing a new habitat for local species.
- → Economical choice using straightforward manufacturing methods.
- → Can be moved by barge.

Disadvantages

→ May allow invasive species to establish and spread.
→ North Sea installations of jacket foundations have reported ongoing grout joint issues, causing long periods of maintenance downtime to sustain structural integrity.
→ Changes to local water patterns may be detrimental to native marine ecosystems.
→ Installations using pile drivers can create underwater noise that may injure or kill some marine life.

Figure 10 *Jacket foundation (public domain).*

Tripod foundations *Figure 11* are designed for use to 50 m, have three-legged tripod bases connected to a cylindrical central column below the waterline. Above the waves, it looks like a monopile. These are different from tri-pile foundations (not discussed here) where three individual pile legs connect to a central support tower above the waterline.

Advantages

→ Seabed site doesn't need advanced preparation before installation.
→ Well-suited for locations where stiff clays or medium-to-dense sands are present, and can be used in softer soils, too.
→ Become an economical choice for installations at 45 m or more.
→ Provides extra stability to the wind turbine.

Disadvantages

→ Scour protection may be needed around the tripod base in locations where bottom currents are significant or where sediment is easily eroded.
→ Tripod construction and maintenance costs can be higher than other base types.

Figure 11 Tripod foundation (image by cathwell.com).

Gravity-Based Foundations

Gravity-based foundations are normally self-buoyant and can be floated or towed out to the location of the offshore wind farm. Since the placement of the gravity-based foundation on the seabed requires a flat area, seabed preparation and scour protection steps are needed. When the seabed is prepared and the foundation is positioned in the right location, the foundation is sunk by the influx of water, and then the base of the foundation is filled with ballast to anchor the foundation. When ballasting is finished, the turbine tower can be directly installed on the topside of the gravity-based foundation.

Designed from precast concrete and suitable for sites to depths up to 30 m, gravity-based foundations (GBFs) *Figure 12* use gravel, sand or stones for ballast.

Advantages

→ Uses lower-cost materials like concrete and steel.
→ Proven technology borrowed from oil and gas industries.
→ Some designs do not need crane installation.
→ Tugboats can move port-assembled floated-to-fixed GBFs into place, reducing costs and risk.

Disadvantages

→ Seabed preparation like dredging is typically required. This can disturb a significant amount (up to 7%) of the wind farm's site.
→ A larger installed footprint may increase the turbine's environmental impact.
→ Invasive species introduction is possible when towing foundations from port to site.
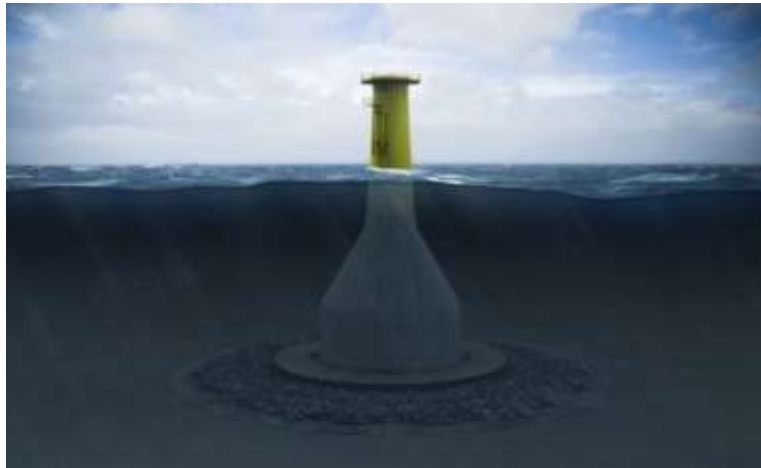
Figure 12 Gravity-based foundation (image by Seatower AS).

Floating Foundations

Floating technology *Figure 13* allow access to deep-water sites where fixed structures are not feasible. It has already been used successfully in places like Scotland and Portugal, with more worldwide projects in development.

Advantages

→ Significantly increases the reach of wind farms, allowing installations to over 200 m.
→ Takes advantage of the 58% of offshore wind resources in deep water located where traditional foundations cannot reach.
→ Turbines and bases can be assembled in port, then towed to site for installation. Longer maintenance can also be done in port, if desired, by towing the turbine back to port.
→ Installations further offshore (at least 10 km) minimizes the risk to migratory birds.
→ Less visual impact on shore.

Disadvantages

→ Cabling to affix the platforms in place requires ongoing inspection and maintenance.
→ Anchors and cabling can disrupt sea life.
→ Because turbines are towed to site, the possibility of invasive species introduction is increased.

Figure 13 Floating foundation (image by windFloat Atlantic).

Turbine installation

The installation activities of the wind turbine include overland transportation of components from the production sites to the harbor, over-water transportation from the harbor to the erection sites, and component assembly by specific installation vessel as mentioned before, and crane.

The tower, nacelle, hub and blades are the turbine components to be installed. It starts with Tower installation. The tower sections are typically assembled at the onshore assembly site at the harbor and the complete tower is transported to the location of the wind farm by the installation vessel. When the installation vessel is in position and stabilized, the tower is lifted and placed on top of the foundation and then bolted. If tower sections are not assembled at the onshore assembly site, the assembly takes place offshore, which logically consumes more time and effort due to the harsh weather conditions offshore.

Followed by tower installation, the nacelle is lifted by the crane off the installation vessel and placed on the top of the tower. In case the blades are not already attached to the nacelle, each blade should be lifted separately and connected to the hub. Then, to not change the vessel or crane position, the rotor is rotated to make space for the installation of a new blade. This operation is iterated up to the moment that all three blades are installed. Usually, turbine installation is limited by a maximum wind speed of 8 m/s and a maximum wave height of 2 m

(Paterson et al. 2018). These values may vary based on several factors (i.e., the pre-assembly method used, and the vessel used for installation).

Substation installation

Proper electrical infrastructure is required to connect the wind turbine generators to a grid. If an offshore wind farm is located near to shore, an onshore substation is sufficient; but if the wind farm is located distant from the shore, both onshore and offshore substations are required. Prior to the installation of an offshore substation, its foundation should be installed. Typical choices for the foundation of an offshore substation are covered on *Section 2.1.3.3*. When the foundation is installed, the complete substation should be lifted from the installation vessel and be placed on top of the foundation.

Cable installation

Cable installation is the last step of the offshore wind farm installation. Array cables connecting the output power of turbines are connected to one or two offshore substation busbars, depending on the size and location of the wind farm. Then, using export cables, the high-voltage electricity produced by the offshore wind farm is transferred to the onshore substation and from there, to the local electrical grid. The array and export cable routes are optimized in order to minimize the total cable length and follow all environmental laws and marine restrictions. Array and export cables installations are discussed below. (Asgarpour,2016)

Array cable installation: The array or infield cables are lines of cables connecting several turbines to an offshore substation. If a monopile foundation is used, the array cables are pulled through J-tubes and then are connected to the wind turbine cables in the tower bottom. After cable pulling, a second layer of scour protection by rock dumping may be applied around the foundation.

The array cables should be placed 1 or 2 m under the seabed in the space between wind turbines. This is done using trenching remotely operated vehicles (ROV) departed from an offshore vessel and monitored by an experienced pilot to not damage the cables. The trenching ROV buries the array cables 1 or 2 m below the seabed, depending on the environmental requirements and IEC and DNV standards (i.e., *DNV-RP-J301 guideline*). The last turbine in a row is connected to an offshore substation. This operation should be done for each row of connected turbines.

Export cable installation: After connecting array cables to offshore substations using transformers, the voltage is stepped up for onward transmission over a longer distance. The export high-voltage AC or DC cables connect the offshore substations to an onshore substation. The installation of export cables is similar to array cables, but larger cable-laying vessels and trenching ROVs are used. Typically, the cables near shore should be buried deeper than those far from the shore. After export cable installation, pre-commissioning tests can be carried out and then, the offshore wind farm can be commissioned.

2.1.3.4 Operation & Maintenance

Maintenance of a wind turbine requires the ongoing services of a team of technicians. The technicians are trained to perform both routine maintenance, day-to-day troubleshooting and more major repairs as required.

Each of the turbines has multiple sensors, typically providing information on vibrations, temperature and oil quality. The turbines have a permanent data connection that goes to a data gathering and monitoring center (CMS) which enables the technicians or engineers monitor the turbine twenty-four hours, seven days a week.

In the event of a performance disruption, the service team either adjusts from the control room or, if necessary, technicians are dispatched to site with precise support instructions.

The two most used maintenance strategies for wind turbines are Reliability-based (or Reliability centred) and Condition-based maintenance.

Both reliability-based and condition-based maintenance aim to find the optimum maintenance point and have some overlap in terms of the approach taken to identify this point. For example, in condition-based maintenance analysis, reliability data is also an important input and reference. Reliability-based is more efficient when components have frequent failures with short downtimes; whereas condition-based maintenance is more efficient when applied to components that seldom fail, i.e. blade shell (I. Dinwoodie et al., 2015), but which result in large downtimes.
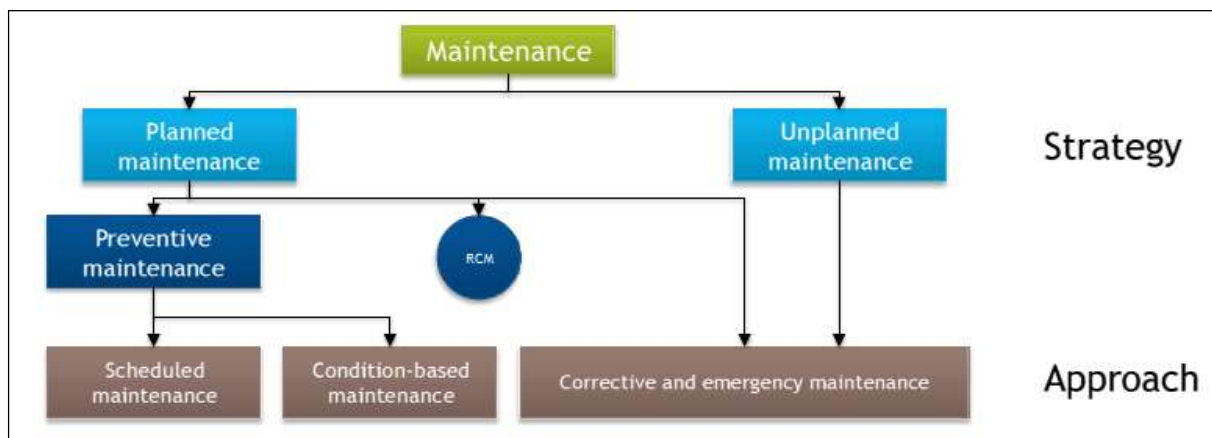
Figure 14 *Maintenance flow chart*

Maintenance activities can be subdivided into preventive and corrective maintenance.

→ **Preventive maintenance:**

- Calendar based maintenance, based on fixed time intervals or on fixed numbers of operating hours.

- Condition based maintenance, based on the actual health of the system. This requires online condition monitoring systems and inspections.

→ **Corrective maintenance:**

- Planned maintenance, based on the observed degradation of a system or component (a component failure is expected in due time and should be maintained before it occurs).

- Unplanned maintenance, necessary after an unexpected failure of a system or component.

→ **Unplanned Maintenance**

Unscheduled maintenance refers to the maintenance activity's that have to be carried out on an ad-hoc basis when a wind turbine went into failure mode. This is the unplanned corrective maintenance displayed in figure above. The aim of every offshore wind O&M strategy should be to reduce this type of maintenance to a level as low as economically reasonable. Unscheduled maintenance causes additional expenses due to the additional downtimes caused by the preparation and reaction period (Time to organize, mobilization time, travel time) and the associated energy production loss. Of course, unscheduled maintenance cannot be avoided completely and always will be a part of every O&M strategy.

→ **Scheduled Maintenance**

Scheduled maintenance (SM) includes all time regular service activities that are required to keep the wind turbine running. Typically, wind turbine blades are subjected to a defined scheduled maintenance program involving a major service in certain time intervals. Commonly this comprises an annual service and a three (3) to seven (7) year major overhauls. This varies between the different original equipment manufacturer (OEM). Project owner strategy and certification requirements supplemented by periodic inspections regimes can further influence the workload. The scheduled maintenance is usually undertaken during the summer month. The average metocean conditions during the summer are more favorable.

→ **Reliability Centre Maintenance (RCM)**

Reliability-based maintenance aims to find the "right" time for maintenance by assessing the state of health of the blade drawing on judgment based on experience of reliability functions.

Table 1 Types of services for WTB

Types of services for Wind Turbine Blades	
Scheduled Maintenance	*Unscheduled Maintenance*
Annual service	Blade inspection and repair
Normal glass fiber repairs	
Structural repairs	
Surface coating	
General cleaning	

2.1.3.5 Decommissioning

In the next decade, it is expected that offshore wind farm decommissioning will surge since many offshore projects commercialized in the early 2000s. Considering the differences in foundation type, weather conditions, seabed conditions, etc., the decommissioning schemes are expected to be exclusive to and unique for each wind farm.

Decommissioning is considered to be the last stage of the life cycle process. According to Welstead et al. (2013), decommissioning can be defined as the reverse of the installation phase; the objective of decommissioning is to return the site to its condition before project deployment as far as possible. In another words, it is the process of dismantling the entire wind farm including removal of the foundations, removal of the WTs and cables, etc.

However, some components of the wind farm usually have a longer lifetime. For instance, a gravity-based foundation can last over 100 years (Bradley, 2014) and the internal array and transmission cables can be used for more than 40 years (Yanguas, 2012). Additionally, a two-year period of monitoring and remediation is required to ensure that the site returns to the state before wind farm construction (Ortegon, 2013). Hence, a repowering optimization approach is suggested since can be a sustainable alternative solution to extend the lifetime of a wind farm besides having a smaller LCoE than the refurbishment approach, process of installing minor components such as rotors, blades, gearbox, etc (Hou, 2017). The wind farm owners would continue to use most of the original electrical system (and/or foundations) to install bigger WTs or change some components, such as drive trains or electronic devices which can improve the production efficiency. It has become an increasing common practice for Germany and Denmark (Goyal, 2010).

2.1.4. Onshore Assembly

The onshore assembly site at the harbor is where, based on the installation strategy, all component assemblies are completed, components are then loaded onto the installation vessel to be transported to the site of the offshore wind farm. There is no assembly required for onshore and offshore substations and typically they are transported to their installation locations. In addition, there is no assembly necessary for foundations and, depending on their manufacturing location, they can be directly transferred to the location of the offshore wind farm. Therefore, assembly at the harbor only applies to wind turbine components. Based on the installation strategy, the following assembly concepts for wind turbine components are possible:

1. No onshore assembly: All components are transported to the location of the offshore wind farm and then installed one by one.
2. Tower assembly: The tower sections (typically three or four sections) are assembled at the onshore assembly site. Then, the whole tower structure is bolted on the deck of the installation vessel to maximize the vessel's loading capacity.
3. Assembly of two blades and the nacelle: The nacelle, hub and two blades are connected together. This concept is also known as the "bunny ear" concept. When the assembly is done, the nacelle with two blades attached is placed on the deck of the installation vessel.
4. Assembly of three blades and the nacelle: This concept is similar to the bunny ear concept, but with the whole rotor is attached to the nacelle. The downsize of this concept is that the required deck area for each rotor-nacelle assembly is huge and assuming existing offshore vessel designs, only one rotor-nacelle assembly can be loaded on the deck. A workaround is to place the rotor-nacelle assemblies on top of each other, which requires the correct structure on the deck for load handling and damage prevention. (Asgarpour,2016)

2.1.5. Offshore Transport

Prior to the installation of an offshore wind farm, the transportation of all components to the offshore wind farm location is done. Depending on the location of the harbor, wind farm and manufacturing facilities, the foundations and offshore substations can be directly transported to the location of the farm. However, wind turbine components are typically transported to the onshore assembly site at the harbor and then are loaded on installation vessels. Currently, there are several installation vessels customized for offshore wind industry and more optimized vessels are in the design phase. Depending on the project specification, one of the following installation vessels can be selected for foundation, substation, and turbine installation:

• Floating vessel stabilized with mooring lines

• Floating vessel equipped with motion-compensated crane

• Jack-up barge

Currently, jack-up barges are used most often for close to shore wind farm locations and floating vessels with motion-compensated cranes are used for deep waters. For array and export cable installation, custom-made vessels are used. These vessels are customized for cable laying, trenching and rock dumping. For each specific project and installation strategy an installation vessel is reconfigured for equipment placement and deck preparation. This step is normally called the mobilization and takes place before loading the components from the manufacturing facilities or the onshore assembly site at the harbor to the deck of the vessel. When the installation is finished, the deck area is reconfigured for the next offshore wind installation. This step is normally called demobilization. Mobilization and demobilization of large installation vessels are costly and time-consuming (each operation can take up to one month). Asgarpour (2016)

The vessel can sail to the location of the wind farm, after the mobilization of the installation vessel and loading the components to the deck of the vessel. It should be noted that sailing out to the location of the wind farm can only take place when the weather conditions at the location of the wind farm are suitable for the next installation step. Otherwise, the vessel will wait at the harbor for suitable weather conditions, but the vessel daily rate should still be paid. This delay is normally known as weather delay and for far offshore wind farms can be a significant project risk. Therefore, it is advisable that, based on the historical weather data, the weather delay per installation step be calculated. If this calculation is done, the optimal starting date for the installation can be found to minimize the total weather delay. (Asgarpour,2016)

2.1.6. Operations & Maintenance of Offshore Wind Farm - Challenges

Offshore repairs are estimated to be five to ten times more expensive than onshore repairs because the former is located farther out into the sea where waters are quite deep (Hofmann et al., 2013; Shafiee, 2015a) making its accessibility more complex. Besides, the limited availability of OWFs. Offshore repairs not only need expensive crane vessels, but they are also dependent on suitable weather conditions, which extends the waiting periods for repairs (Breton and Moe, 2009; Utne, 2010).

Over the entire lifecycle of offshore wind farms, O&M account for around 20-35 per cent of the total energy costs in this sector (Shafiee, 2015a; Ortegon et al., 2013). Baagøe-Engels et al. (2016), have highlighted several challenges for O&M in the offshore wind energy sector.

These challenges can be grouped into four categories:

→ Issues related with industry immatureness
→ Distance and water depth
→ Weather window
→ Policy issues

Three other major issues that lead to increased O&M costs were identified by The Delphi technique which uses interactive feedback loops with a group of experts and has been applied in different fields, such as operations management, sustainable supply chain management and IT governance implementation (Baagøe-Engels et al., 2016):

→ Too many predefined rules that limit development
→ Lack of coordinated planning of the different services offered at the wind farms
→ Lack of a common approach on how O&M should be managed strategically

More information on the challenges categories and The Delphi technique described above can be found on Baagøe-Engels et al. (2016).

3. Basic Theory

The analysis and presentation of the underlying literature is divided into three parts to follow the subject matter of this project: an overview of OWF history, going through its project development until its decommissioning, presented in **Section 2,** offshore wind profile & power performance methods (HHWS and REWS) that will be discussed in the following sections.

3.1 Offshore Wind Profile

In the offshore regime, external wind conditions are determined in guidelines by International Electrotechnical Committee (IEC), Det Norske Veritas (DNV), and Germanischer Lloyd (GL).

→ IEC 61400-1. Wind Turbines – Part 1: Design Requirements, 2005
→ IEC 61400-3: Wind Turbines – Part 3: Design Requirements for Offshore Wind Turbines, 2009
→ DNV-OS-J101: Design of Offshore Wind Turbine Structures, 2014
→ DNV-RP-C205: Environmental Conditions & Environmental Loads, 2010
→ DNV-RP-J101: Use of Remote Sensing for Wind Energy Assessments, 2011
→ GL Guideline for the Certification of Offshore Wind Turbines, 2005

Standards relevant to offshore technologies have been developed by The American Petroleum Institute (*API 2000*) and the International Standards Organization (*ISO 2004*). They do not specifically address offshore wind turbines; however, guidelines are provided for the design of offshore structures in general, particularly with regards to structural integrity. The *API* and *ISO* guidelines are mentioned here for completeness but are not discussed in detail.

As stated in the standards, ideally the wind conditions should be determined from measurements at the site in question. The site conditions should then be correlated with long-term records from local meteorological stations. In order to obtain reliable parameters, the measurement period should be sufficiently long as mentioned in the *IEC standards*, but no time period is specified. The *GL guidelines* specify that a minimum measuring period of 6 months is required. However, if seasonal variations contribute significantly to the wind conditions, then the measurement period should account for this. A 10-years period or more of continuous data with sufficient time resolution is recommended for design the wind climate database by *DNV-RP-C205*. If a long term measurements is not available, they suggest that

the wind velocity climate can be estimated from hindcast wind data and *DNV-RP-C205* mentions the World Meteorological Organization (WMO 1983) to obtain the minimum requirements to hindcast models and their accuracy. With regards to DNV-OS-J101 standard, they suggest that a 10 min mean value of wind speed should be obtained from several years of data.

In all standards, the wind speed at 10 m is often used as the reference height. In case wind speed data are only available for heights other than the reference height, an assumption of the wind profile is to be done. This assumption is used to define the average vertical wind shear across the rotor disk. The wind shear can be affected by different factors such as friction velocity, roughness length and atmospheric stability.

The wind speed profile may be represented by an idealized wind profile in a non-complex terrain and atmospheric conditions. The standards recommend different wind profile models to determine the vertical structure of the Marine Boundary Layer (MBL). *Figure 15*
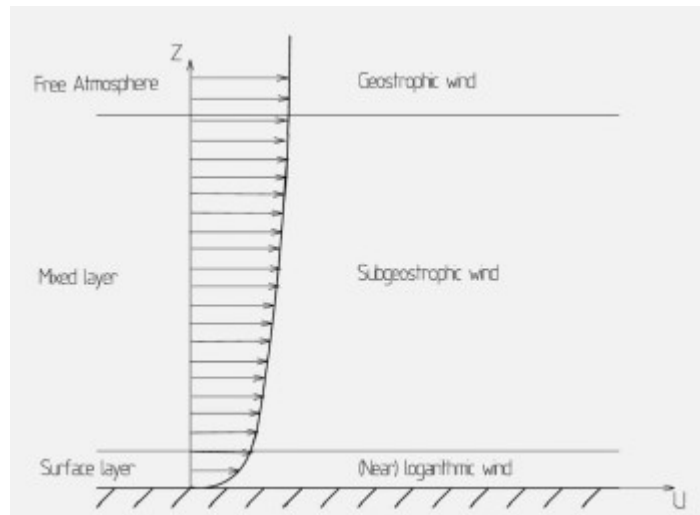
Figure 15 Typical wind profile in the Marine Boundary Layer

A brief description of the conventional wind profile extrapolation models is given below, including the power law considered in this study.

3.1.1. Power law profile

The wind profile $\underline{U}(z)$ denotes the average wind speed as a function of a reference height z above the ground. In the GL standards, the normal wind speed profile is assumed to be given by the power law:

$$\overline{U}(z) = \overline{U}_{ref} \left(\frac{z}{z_{ref}} \right)^{\alpha}$$

[1]

The power law has no explicit theoretical basis and is just a function known to fit the logarithmic wind profile. This profile is widely used in engineering applications because it is easier to work with a power law than with the logarithmic wind profile. This method does not take into account the roughness effects due to waves and thermal effects due to atmospheric stability (Obhrai et al. 2012).

After rearrangement of the equation above:

$$Log \left(\frac{\overline{U}(z)}{\overline{U}_{ref}} \right) = Log \left(\frac{z}{z_{ref}} \right) * \alpha$$

$$\alpha = \frac{log \left(\frac{\overline{U}(z)}{\overline{U}_{ref}} \right)}{Log \left(\frac{z}{z_{ref}} \right)}$$

[2]

$\overline{U}(z) -$ is the wind speed (m/s) to be calculated at height z;
$\overline{U}_{ref} -$ is the known wind speed (m/s) at height z_{ref};
$z -$ is the height (m) above ground level for wind speed;
$z_{ref} -$ is the reference height (m) where $\overline{U}_{ref}$ is known;
$\alpha -$ is the wind shear exponent.

Wind shear is quantified as the exponent α (alpha) in the power law equation that relates wind speeds at two different heights. The shear calculations are performed only where valid upper and lower wind speed measurements are available for a given time interval. In practice, it has been found that α varies with such parameters as elevation, time of day, season, temperature, terrain, and atmospheric stability. The larger the exponent the larger the vertical gradient in the wind speed.

Although the power law is a useful engineering approximation of the average wind speed profile (Peterson and Hennessey, 1978; Wharton and Lundquist, 2012b; Vanderwende and Lundquist, 2012; Emeis, 2013), wind profiles may differ from a logarithmic profile across the rotor diameter of a turbine (Wagner et al., 2009). Besides, α does not consider veering or backing or even the magnitude of the wind speed.

3.1.2. Logarithmic profile

The logarithmic wind profile is given as:

$$\underline{U}(z) \;=\; \left[\frac{u_*}{\kappa}\right] ln \left[\frac{z}{z_0}\right] \qquad\qquad [3]$$

Where $\underline{U}$ is the wind speed (m/s), κ is the von Karman constant (typically taken to be 0.4), z is the height (m) above surface, u_* is the friction velocity, and z_0 is the aerodynamic roughness length (m). The roughness length can be considered as the point where the wind speed becomes zero when extrapolated towards the surface using Monin-Obukhov theory (Stull 1988b). This dependence is expressed by:

$$z_0 \;=\; \frac{A_c u_*^2}{g} \qquad\qquad [4]$$

where g is the gravitational acceleration (m/s2) and the empirical constant A_c is the Charnock constant.

The *DNV-OS-J101* standard suggests logarithmic wind speed profile for neutral atmospheric conditions within the lowest section of the surface boundary layer. As an alternative to the logarithmic profile, the *DNV-OS-J101* guideline also suggests the power law in equation [1].

Under conditions of stable stratification, the logarithmic assumption has been shown to break down at rotor-swept heights as turbulent fluxes decrease in magnitude and near-surface winds begin to decouple from the winds aloft (Optis et al., 2014, 2016). Under such conditions, phenomena such as low-level jets can occur, which idealized models, such as the logarithmic wind profile—which assumes monotonically increasing wind speeds with height—are unable to account for.

3.1.3 Logarithmic profile with stability correction

Since the validity of wind profile estimators is affected by the atmospheric stability, an adjustment is made to the estimator formula to achieve the appropriate value under different stability conditions, *DNV-RP-C205* standard. Stability corrections wind profile are made from the logarithmic wind profile in Equation [3] with an added stability correction term. A relationship between wind speeds at different heights with stability corrections principle is given below:

$$\underline{U}(z) \; = \; \frac{u_*}{k}\left[ln\left(\frac{z}{z_0}\right) \; \pm \; \psi_M\left(\frac{z}{l}\right)\right]$$

[5]

in which ψ_M is the stability function for momentum that adjusts the wind profile depending on atmospheric stability, and L is the Monin-Obukhov length that characterizes surface layer atmospheric stability.

$\boldsymbol{\psi_M}$ **> 0** – Stable conditions

$\boldsymbol{\psi_M}$ **< 0** – Unstable conditions

$\boldsymbol{\psi_M}$ **= 0** – Neutral conditions

The stability function ψ_M depends on the height z and the Monin-Obukhov length l. The *DNV-RP-C205* guideline references (Stull 1988b) for the relevant expressions between ψ_M and L. It is stated that the Monin-Obukhov length L can be calculated using the Richardson number R, a dimensionless parameter whose value determines whether convection is free or forced and it is expressed below:

$$R \; = \; \frac{g\dfrac{d\varrho_0}{dz}}{\varrho_0\left(\dfrac{dU}{dz}\right)^2}$$

[6]

g is the gravitational acceleration (m/s2);
ρ_0 is the undisturbed density (sg);
$d\rho_0/dz$ is the vertical density gradient;
dU/dz is the vertical gradient of the horizontal wind speed.

The *DNV-RP-C205* guideline suggests that the Richardson number can be computed from averaged conditions by the method described in Panofsky and Dutton (1984) in case data for the Richardson number R are not available.

3.2 Atmospheric Stability

It refers to the tendency for air parcels to move vertically, either to rise or sink depending on its temperature relative to the surroundings. The environment is characterized in terms of its static stability which determines whether an air parcel remains buoyant or not. When the temperature of the air parcel is greater than the temperature of the surrounding environment, then it will continue to rise (unstable case). And when the temperature of the surrounding parcel is less than the surrounding environment, then it will continue to sink (stable case). In neutral condition, it will stay where it is.

Buoyancy-generated turbulence is often referred as the turbulence due to atmospheric stability. It is to be noted that the term 'turbulence' refers to summation of mechanically and

buoyancy-generated turbulence, unless otherwise stated. The atmospheric stability can be classified into three classes:

Stable condition: *Less vertical mixing, more velocity shear, i.e. a higher velocity gradient.*

Neutral condition: *Constant temperature with height (H). No wet buoyancy.*

Unstable condition: *More vertical mixing, less velocity shear, i.e. a lower velocity gradient.*
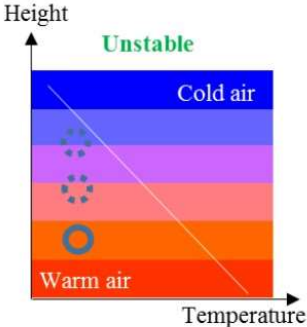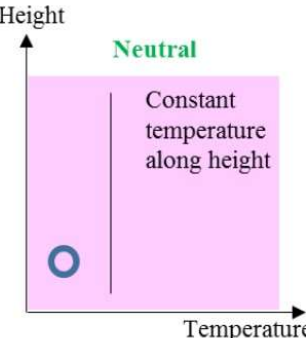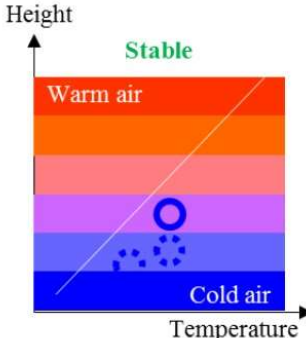
Height — Unstable	Height — Neutral	Height — Stable
Cold air / Warm air — Temperature	Constant temperature along height — Temperature	Warm air / Cold air — Temperature
• Also known as buoyant turbulence • Negative temperature gradient • Positive buoyancy, warm air parcels continue to rise to a level where the temperature is equal, causing instability • The rising air expands and cools down as the atmosphere pressure drops • More vertical mixing, more vertical turbulence or buoyancy-generated turbulence • Less velocity shear, lower velocity gradient	• No net buoyancy, air parcels remain at its level	• Also known as buoyant suppressed turbulence • Positive temperature gradient • Negative buoyancy, cold air parcels continue to sink to a level with equal temperature, causing stability • The sinking air compresses as the atmosphere pressure increases • Less vertical mixing, the turbulence is stratified in each layer • More velocity shear, higher velocity gradient

Figure 16 Main differences between the atmospheric stability classes (Putri, 2016).

Cooling and heating of the surface of the earth takes place causing different stratification, throughout the day. Net heat flux to the ground determines the stability, resulting from the incoming solar radiation and outgoing thermal radiation, and of latent and sensible heat exchanged with the air and subsoil. *Figure 17*

Onshore, the atmospheric stability is a diurnal cycle where stable condition normally occurs at night, when cooling of the earth`s surface reduces the vertical temperature gradients and unstable condition during the afternoon, when warming of the earth`s surface increases the vertical temperature gradients.

Offshore, the atmospheric stability is a seasonal cycle where stable condition normally occurs during the springtime, when the air temperature is often warmer than the sea surface temperature and the unstable condition takes place usually in the winter time, when the air temperature is often cooler than the sea surface temperature.
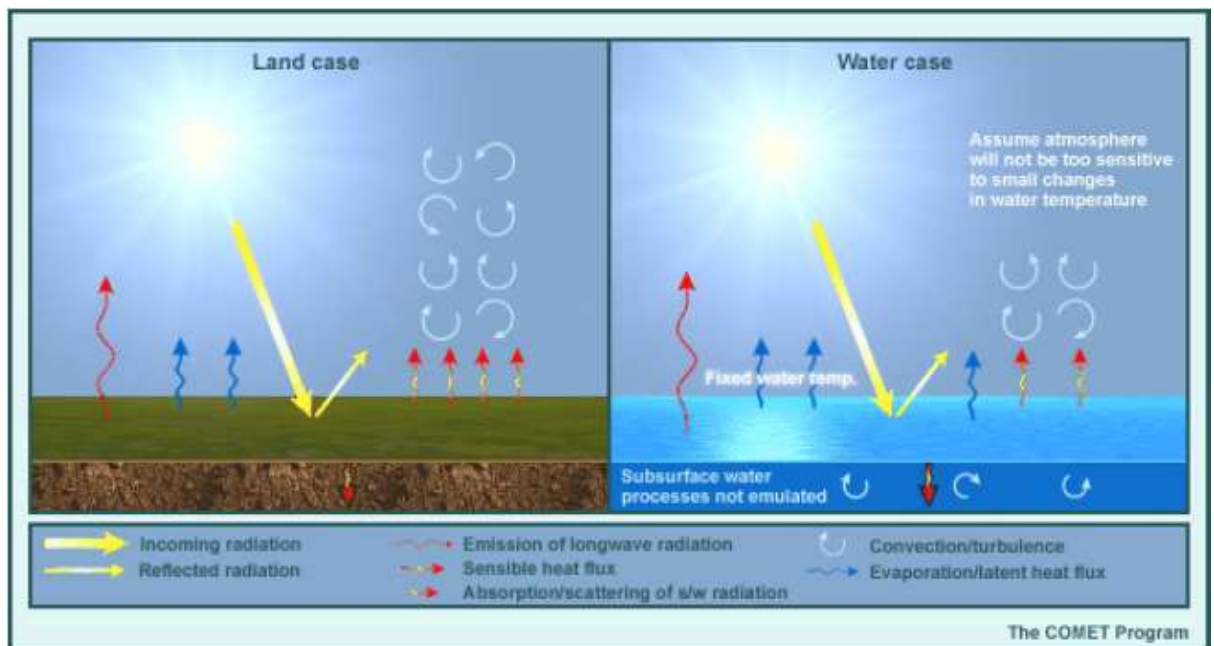
Figure 17 Difference in Energy balance onshore and offshore

(source: http://www.meted.ucar.edu/nwp/model_physics/print.htm)

As described in *Figure 16* , buoyancy-generated turbulence contributes to air parcel mixing between air parcel layers. For unstable conditions, it decreases the velocity shear gradient and the opposite effect occurs under stable conditions where more velocity shear occurs, implying abrupt change in wind speed with respect to height (Roy & Sharp, 2013).
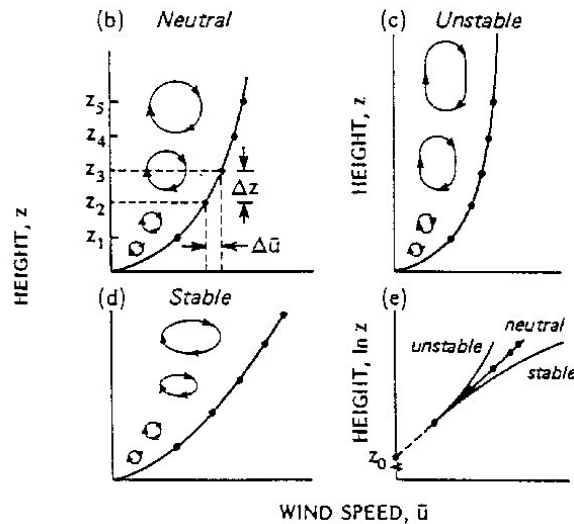
Figure 18 *Atmospheric stability effect to the mean wind speed profile/wind shear (Thompson, 1979).*

It is important to know the change in velocity (wind shear) over the rotor swept area specifically for multi-mega modern wind turbines because higher wind shear value will result in a larger cyclic loading on the blades.

3.3 Current research

The wind profiles described in *Section 3.1*, the standard logarithmic in *equation 3* and power law in *equation 1*, assume homogeneous and neutral wind conditions. Throughout a comparison of average wind velocity profiles measured offshore at the FINO1 research platform with the vertical wind profile computed using power law as recommended in the *IEC 6400-3* (2009) and *GL* (2005) *standards*, Neumann, Emeis, and Illig (2007) showed that the predicted power law profile can underestimate wind speed under stable conditions, particularly at heights above 40m. According to Lange et al. 2004; Motta, Barthelmie, and Vølund 2005, offshore wind profiles can be governed more by atmospheric stability rather than roughness parameter z_0 and that including the stability effects into the standard logarithmic profile in *equation 3* leads to an improvement of the vertical wind profile predictions, with a general consensus in the scientific literature.

Deviations from the standard logarithmic profiles for all thermal conditions were showed by Tambke et al. (2004) for the measured wind profiles at Horns Rev and FINO1. Land sea discontinuity effects were discarded once these observations were seen for long fetches up to 800 km. Instead, they have suggested that the observed deviations were the result of a decrease in the height of the atmospheric boundary layer due to lower turbulence in the offshore marine environment, concluding that the upper instruments could be in the Ekman layer where surface theory and hence a logarithmic profile is no longer valid. An alternative method to model the vertical wind profile which is based on the inertial coupling between the Ekman layer of the atmosphere and the ocean with constant shear stress in between was proposed.

Using long term data, 4 years, from three Danish offshore meteorological masts to study the role of the stability on the marine vertical wind profile, Motta, Barthelmie, and Vølund (2005) showed that a change in velocity of up to 50% from the original value was obtained when applying the stability corrections to very stable conditions. The fetches at each of these masts varied from 2 km up to 100 km. Since two of the masts (Vindeby & Rødsand) were near to the coast, there was evidence of a land sea discontinuity under certain wind directions, but this was not further studied. Lange et al. (2004) also noticed wind profiles which deviated from the standard logarithmic profile while carrying out a study of the wind climate at Rødsand, showing that the discrepancies were observed under conditions of warm air advection over a colder sea surface, even for fetches up to 30 km. They have suggested that in coastal waters warm air advection is a frequent occurrence which will have an important effect on the average wind profile. However, no alternative methods were suggested to model the vertical wind profile under this type of condition.

A review on the current state of the art in offshore wind modelling were carried out by Obhrai et al. (2012) where gaps between best knowledge and best practice were highlighted. Using FINO 3 data, Eliassen et al. (2012) carried out an investigation related to the impact of stability on the fatigue of an OWT, showing that when considering stability, there is an increment of 40% on the fatigue loading at the root of the blades.

Optis et al. (2014, 2016) analyzed that the logarithmic assumption has been shown to break down at rotor-swept heights under conditions of stable stratification as turbulent fluxes decrease in magnitude and near-surface winds begin to decouple from the winds aloft. Phenomena such as low-level jets can occur, under such conditions, which idealized models, such as the logarithmic wind profile—which assumes monotonically increasing wind speeds with height—are unable to account for (Optis et al., 2014, 2016).

After carrying out an extensive study between the most common wind profiles described on this paper for a wind farm installation campaign simulation, using same amount of data (9-years - Sept 09 to Aug 18) from FINO 3 research platform, Afolarinwa David (2019) concluded that the power law (0.12 & 0.14 exponent) and logarithmic wind profiles model data may underestimate the number of available winds as expected. A new approach based on the extended wind profile (Gryning's boundary layer shear profile) was suggested, showing that this new approach performs well for stable conditions except for very low wind speeds where it underestimates the wind speed. For unstable conditions, it was also shown that the extended wind profile performs well for wind speed above 14 m/s but for lower wind speed it underestimates the wind speed (Afolarinwa David, 2019).

A more recent study related to new methods for improving the vertical extrapolation of near-surface offshore wind speeds, Optis et al. (2021) contrasted the conventional logarithmic profile against three novel approaches: a single-column model, a logarithmic profile with a long-term stability correction and a machine learning model. Models were developed and validated using 1-year of observations, wind speeds reported at every height from 20-200 m, from two floating lidars deployed in United States Atlantic offshore wind energy areas. They found that the machine learning, a relatively simple ensemble-based regression tree method, known as a random forest model, significantly outperforms all other models across all seasons, stability regimes and times of day. Machine-learning model performance is considerably improved by 10 including the air-sea temperature difference, which provides

some accounting for offshore atmospheric stability. Finally, there was no degradation in machine-learning model performance when tested 83 km from its training location, suggesting promising future applications in extrapolating 10-m wind speeds from spatially resolved satellite-based wind atlases. This model has shown strong predictive power in previous land-based wind speed extrapolation work (Bodini and Optis, 2020a, b) and in relating wind plant energy production to on-site atmospheric variables (Optis and Perr-Sauer, 2019).

3.4 Turbulence

In the ABL, turbulence is either generated by shear or by thermal instability. Thermal production of turbulence is dominant for lower wind speeds, but it becomes nearly negligible for high wind speeds when compared to shear production. Onshore, the shear production is dependent exclusively on the surface roughness and is assumed to be independent from the atmospheric conditions. However, surface roughness increases with wind speed, thus increasing wave height for offshore conditions.

3.4.1 Turbulence Intensity

Power curves of WTs are influenced by turbulence intensity, a dimensionless number defined as the standard deviation of the wind speed divided by the mean wind speed for a particular time step. A significant part of the turbulence intensity effect is caused by the averaging of the measured power output and the measured wind speed over 10-min periods. This can be understood from the non-linear relationship between the power output and the wind speed *IEC 61400-12-1 standard*.

Assuming a homogeneous terrain, i.e. homogeneous turbulence in the horizontal plane, the statistical characteristics of turbulence change only with height. For offshore conditions, the turbulence intensity increases with wind speed.

In NORSOK N-003 standard, the turbulence intensity is given as a function of height according to a "power law" with the exponent of -0.22:

$$I_u(z) = 0.06\,[1 + 0{,}043\,U_0]\,(\tfrac{z}{z_0})\wedge - 0.22 \qquad\qquad [7]$$

$I_u(z) -$ is the turbulence intensity factor;
$U_0 -$ is (m/s) is the 1-h mean wind speed at 10m;
$z -$ is the height (m) above sea level for wind speed;
$z_0 -$ is the reference height (10 m);

Note: Unless a more detailed assessment is made, the average wind velocity at 10 m above sea level with an annual probability of exceedance of 10^-2 can be chosen as U_0= 36m/s (1-hr average) for the whole continental shelf. The characteristic value with an annual probability of exceedance of 10-4 can be chosen U_0 = 41 m/s (1-hour average).

3.5 Data normalization

3.5.1 Wind Shear & Wind Veer

The inflow across the turbine rotor disk is not necessarily represented by hub-height wind speeds and directions. Wind speed and direction can vary with height across the rotor area, a phenomenon known as shear. "Wind shear" is related to the change in wind speed with height whereas a change in wind direction is considered "wind veer" (Holton, 1992). The direction of the change in wind direction can also be useful, in atmospheric science; in the Northern Hemisphere, clockwise rotation with height is considered "veering", while counterclockwise rotation is considered "backing."

Vertical wind shear or veering or backing over the depth of a turbine's rotor disk are caused by several common atmospheric phenomena. As the effects of surface friction decrease, wind speeds tend to increase with height in the atmosphere. More shear can be experienced over the land than the ocean due to friction.

Shear and turbine power production have been studied over the past 3 decades. In 1990, shear affected power curves, as seen in observations of three 2.5MW turbines (Elliott and Cadogan, 1990). Compared to no shear cases, shear decreases the power coefficient for multimegawatt turbines (Albers et al., 2007). Observational studies found by Walter et al. (2009) showed that an increase in power of a theoretical wind farm using shear values (rather than no shear values) could be of up to 0.5%, while decreases in power could reach 3%.

Wind speed shear and wind directional veer combined effects on a turbine's power production are often stronger than either directional veer or speed shear alone but speed shear showed to exert more influence than directional veer in most circumstances (Patrick Murphy et al., 2020).

3.5.1.1 Wind Shear Representation

The rotor equivalent wind speed concept (object of this literature) accounts for the vertical wind shear and more details are described on *Section 3.6.2*.

3.5.1.2 Wind Veer Representation

The simplest metric to account for the directional veer is βbulk, which considers only differences in wind direction at the top and bottom of the rotor area (Patrick Murphy et al., 2020). The formula is presented below:

$$\beta_{bulk} = (\theta_{top} - \theta_{bottom}) / (z_{top} - z_{bottom}) \qquad [8]$$

Θ_{top} − hub height measured horizontal wind direction at the top of the rotor disk;
Θ_{bottom} − hub height measured horizontal wind direction at the bottom of the rotor disk;
z_{top} − is the highest tip height (m);
z_{bottom} − is the lowest tip height (m);

βbulk resembles depictions of layer-wise directional veer in hodographs (MacKay, 1971), where the shear is only considered as a bulk quantity. Bulk value can be either negative or positive.

Negative βbulk - *It implies backing of the wind across the turbine rotor disk (the wind rotates counterclockwise as it increases in height).*

Positive βbulk - *It implies veer (the wind rotates clockwise as it increases in height).*

While carrying out a simulation, Wagner et al. (2010) found that an increase of the turbine power production is given by a clockwise veer while counterclockwise backing decreases the power produced due to the differences in angle of attack for the turbine blades. However, Sanchez Gomez and Lundquist (2020) noticed the opposite during an observational study such that veer led to a larger decrease on turbine power production than backing.

3.6 Power Performance Measurements

3.6.1. Power Production

The power performance of a wind turbine is represented by its power curve, which states the electrical power production as a function of wind speed

$$P = \frac{1}{2}\rho AV^3 C_P$$
[9]

P is the electrical power (W);

ρ is the air density (kg/m^3);

A is the complete area swept by the rotor (i.e. πR^2 with Radius R);

V is the instantaneous wind speed (m/s);

C_P is the power coefficient.

The procedure to measure a power curve is defined by the international standard *IEC 61400-12-1*. The wind speed takes place at some distance in front of the wind turbine using a cup anemometer located on a meteorological mast (MetMast) at turbine hub height, here defined as the hub height wind speed (HHWS). The underlying assumption is that the hub height measurement is representative of the wind across the entire rotor area. While this assumption was adequate for the size of wind turbines designed and manufactured at the time

that the concept was conceived, rotors of modern multi-megawatt wind turbines span across a large area which may include significant differences in wind flow.

The electric power is dependent on the wind speed cubed, making the power production very sensitive to small variations in the wind speed. Thus, it is important to use a representative wind speed in power curve validations.

3.6.2. Rotor Equivalent Wind Speed Concept

The rotor equivalent wind speed (REWS) metric proposed by Wagner et al. (2009), now advocated in the second edition of the *IEC 61400-12-1* standard, can describe the actual momentum experienced by a turbine rotor area by accounting for the vertical shear.

This concept aims to represent the kinetic energy flux through the entire rotor disk via an equivalent wind speed. This method portrays more accurately the flow through the rotor plane, in particular in wind conditions with non-standard shear profiles, than the HHWS method where the wind speed only at one single height is used. A RDS is recommended in addition to meteorological masts.

$$v_{eq} = \left(\sum_{i=1}^{n_h} v_i^3 \frac{A_i}{A} \right)^{1/3} \qquad [10]$$

n_h is the number of available measurement heights ($n_h \geq 3$);

v_i is the 10 min average wind speed measured at height i;

A is the complete area swept by the rotor (i.e. πR^2 with Radius R);

A_i is the area of the i th segment, i.e. the segment the wind speed v_i is representative for.

The segments (with areas Ai) shall be chosen in the way that the horizontal separation line between two segments lies exactly in the middle of two measurement points. The segment areas are then derived according to

$$A_i = \int_{z_i}^{z_i + \perp} c(z)\, dz$$

where z_i is the height of the ith segment separation line, numbered in the same order as v_i (either top down or bottom up);

$c(z) = 2\sqrt{R^2 - (z - H)^2}$ with R the rotor radius and H the hub height.

3.6.3 Definition of Rotor Equivalent Wind Speed under consideration of wind veer

To account for the wind veer as well (Wagner et al., 2010; Choukulkar et al., 2015; Clack et al., 2016), an angle term (phi) is added to the *Equation 10* above. The REWS formula is re-defined as:

$$v_{eq} = \left(\sum_{i=1}^{n_h} (v_i \ \cos{(\varphi i)})^\wedge 3 \frac{A_i}{A} \right)^{1/3} \tag{11}$$

φi is the angle difference between the wind direction at hub height and segment i;

As defined on the *Equation 11* above, the REWS is influenced by the difference of wind direction measurements at different height relative to hub height. It is important to measure the wind directions at the various height levels with same type of sensor, i.e. one RSD measuring all heights, or same sensors on the meteorological mast at all heights, in order to provide accurate measurements of the difference of wind directions.

3.6.4. Currently Research

Using a blade element momentum model to simulate a 3.6MW turbine, Wagner et al. (2008) show that power production correlates better with the REWS than with the hub-height wind speed. Wagner et al. (2009) found that when considering three or five different heights using the REWS method, the power output was improved. Later work specified a REWS, which considers both speed shear and directional veer (Wagner et al., 2010; Choukulkar et al., 2015; Clack et al., 2016). Wagner et al. (2010) additionally find that directional veer was less influential on the power production than speed shear. In 2014, Wagner et al. found an insignificant influence of wind shear while testing the REWS method at one site for a 500-kW wind turbine (H = 36 m, D = 41 m). Pedersen (2004) also observed that the power production is dependent on the magnitude of the shear and whether the shear is based on direction or velocity. Sanchez Gomez and Lundquist (2020) suggest a combination of directional veer and shear should be considered.

Using the measured HHWS for a 5MW turbine with a meteorological mast and a LiDAR at flat terrain during a 1-month measurement campaign, Wächter et al. (2009) showed that the power curves had good response. When using the REWS, Dupont et al. (2012) could show that the scatter of measurements around a fitted power curve is lower when compared to the wind speed at hub height. After a yearlong measurement campaign, Antoniou et al. (2009) concluded with the notion that the REWS method is to be recommended.

For an offshore site, Westerhellweg et al. (2010) found that the power performance test was improved with the REWS approach. Bardal et al. (2015) resalted that the scatter of the power curve should be reduced when using the REWS approach, although the REWS approach actually only marginally decreased the scatter in the power curve when they performed observation analyzes using a 3 MW turbine during a 10 - month measurement campaign.

A new expression for equivalent wind power has been derived by Choukulkar et al. (2015), capturing the effect of turbulence on available wind power content. Using this equivalent wind power equation, the effect of wind shear, turbulence intensity, direction shear and direction fluctuations on available wind power are estimated. It was observed that, using the new formulation, the wind direction shear has also a significant impact on the available wind power. In addition, this equation allows estimation of the combined effect of various turbulence parameters. Percentage differences in the available power calculated using the new formulation and that from Wagner et al. (2009) is observed to be 1.3% on average in presence of wind direction shear (Choukulkar et al., 2015).

Although former studies used REWS and similar metrics to explore the impact of shear and atmospheric stability on the prediction of power production from megawatt scale turbines (Elliott and Cadogan, 1990; Rohatgi and Barbezier, 1999; Pedersen, 2004; Sumner and Masson, 2006; Albers et al., 2007; Van den Berg, 2008; Antoniou et al., 2009; Walter et al., 2009; Belu and Koracin, 2012; Wharton and Lundquist, 2012b; Vanderwende and Lundquist, 2012; Sanchez Gomez and Lundquist, 2020; Vahidzadeh and Markfort, 2019), a more recent study (Sark et al., 2019) concludes that turbines in regions with flat terrain do not benefit from using REWS rather than a hub-height wind speed.

Finally, Wilfried et al. (2019) concluded that the relevance of REWS approach depends on turbine dimensions, i.e., the ratio of rotor diameter (D) and hub height (H), as well as on the wind shear coefficient (α) at the wind turbine site. They recommend first estimate the wind shear coefficient at the particular location and based on the results, decide for the use of an extra RSD system next to an already installed meteorological mast. For D/H larger than 1.8 and wind shear coefficient values out of the range $-0.05 < α < 0.4$, REWS is recommended. In fact, up to realistically large D/H ≤ 1.8 and $-0.05 < α < 0.4$, the ratio U_{eq}/U_h is within ±1% of unity. Specially at offshore conditions, the effect of non-constant wind shear coefficient is limited to also about 1% Wilfried et al. (2019).

4. Observation data Overview

To develop and validate the power law extrapolation model, we leverage measurement data from three different masts locations, Forschungsplattform in Nord und Ostsee (FINO 1 & 3) and Frøya on the western coast of Norway, Trondelag, with a total of 14, 9 and 6 years of weather data, respectively, being described on *Sections 4.1.1, 4.1.2 and 4.1.3*.

4.1. Research platforms – FINO

FINO stands for Forschung In Nord und Ostsee (Research at North and Baltic Sea) and it is coordinated by the German Federal Environmental Ministry. This research aimed to deploy research platforms close to future offshore wind farms with the purpose to investigate the environmental offshore conditions as well as creation of comprehensive meteorological, hydrographical, technical and biological data base (Beeken & Kindler, 2011). Below, technical facts of the FINO research platforms, including the ones (FINO 1 & 3) being covered by this study.

Table 2 FINO Research Platform technical facts (Beeken & Kindler, 2011).

Research Platform	Location	Commissioning	Height (m)	Water depth (m)	Distance from coast (km)	Foundation	Platform size (m^2)
FINO 1	North Sea	September 2003	101	28	45	Jacket	16*16
FINO 2	Baltic Sea	May 2007	101	24	31	Monopile	12.2*12.2
FINO 3	North Sea	August 2009	120	23	80	Monopile	13*13

4.1.1 Dataset – FINO 1

FINO 1 is located at North Sea, approximately 45 kilometers to the north of Borkum, in water depth of ~30 meters. It was brought into service in the autumn of 2003.

The first German offshore wind farm, site of Alpha Ventus, consisting of twelve wind turbines which have been generating power since April 2010, is in the immediate vicinity.

The mast has 103 m height and consists of cup anemometers, ultrasonic anemometers, wind vanes and temperature measurements. The wind is measured at 8 different heights from 33 m to 100 m as shown in Figure 19. The buoy and AWAC are measuring the wave height, wave direction, and wave peak period with 30 minutes and 1-hour period.

The measurement setup is arranged according to FINO 1 mast shape which is a square cross-section. Cup anemometers are installed on booms on the south-east side of the mast, while the main wind direction is south-west. Wind vanes and ultrasonic anemometers are installed on the opposite north-west side of the mast, as can be seen in Figure 19 as well. Mast and booms dimensions described in Table 3.

FINO 1 platform is monitored centrally from onshore meaning that it operates with no permanently stationed personnel. The platform can be accessed by helicopter or ship. The platform is provided with a helipad to ensure the maximum possible time window for access to the platform, even in poor weather conditions.

Table 3 FINO 1 masts and booms dimensions (Westerhellweg et al., 2012).

Anemometer, height LAT	Mast width	Boom length	Orientation	Ratio (distance to mast centre/mast width)
(m)	(m)	(m)	(°)	(-)
cup 91.5	1.375	3	135	2.7
cup 81.5	1.754	3	139	2.2
cup 71.5	2.124	4	143	2.4
cup 61.5	2.504	5.5	142	2.7
cup 51.5	2.875	5.5	140	2.4
cup 41.5	3.254	6.5	142	2.5
cup 34	3.532	6.5	143	2.3
sonic 81.5	1.754	3	311	2.2
sonic 61.5	2.504	5.5	308	2.7
sonic 41.5	3.254	6.5	308	2.5
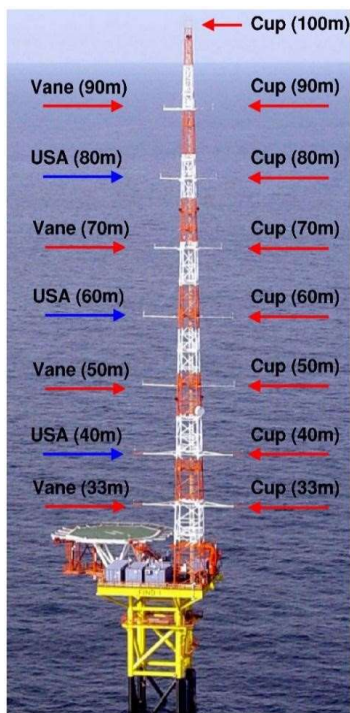
Figure 19 FINO 1 offshore research platform instruments (Ernst & Seume, 2012)

Figure 20 FINO 1 cup anemometer (Bundesamt für Seeschifffahrt und Hydrographie, 2018).

Three conical shells that moves around a vertical axis upon on wind speed that blows through it compose the cup anemometers. The rotation is transmitted to the axis and converted into an electrical signal. This instrument is operating at 1 Hz, capturing the wind speed once every second. A picture of the cup anemometer and its technical specifications can be seen in *Figure 20* & *Figure 21* and *Table 4*.

Table 4 FINO 1 cup anemometer specifications

(Bundesamt für Seeschifffahrt und Hydrographie, 2018)

FINO1 cup anemometer technical specifications	
Manufacturer	Vector Instruments
Measuring range	Type A100LM up to 75 m / s
	Type A100LK up to 150 knots
Resolution	Distance constant 2.3 m + - 10%
	Type A100LM 0.1 m
	Type A100LK 0.0515 m
Measuring interval	1 Hz
Log interval	1 min
Height	**Orientation to boom from the mast**
101 m LAT	Top
91.5 m LAT	135 °
81.5 m LAT	139 °
71.5 m LAT	143 °
61.5 m LAT	142 °
51.5 m LAT	140 °
41.5 m LAT	142 °
34 m LAT	143 °

Figure 21 *Vector instruments A100 series cup anemometers (Windspeed Limited, 2018).*

Ultrasonic anemometer is another instrument on the mast that captures wind speed at three different heights (40, 60 & 80m) and it is located on the opposite side of the mast to the cup anemometer as shown in *Figure 22*. This instrument operates by using 3 sound transmitter and receivers which are aligned in pairs opposite to each other into three spatial directions. The transmitted sound waves are displaced by the wind and reach the receiver with a certain time delay. The horizontal wind speed and wind direction are calculated from the wind speeds along the three-spatial axis by derivation from the time delay. The ultrasonic anemometer has higher measurement frequency at 50 Hz, meaning that it captures 50 times wind speed every second and is expected to have more precise measurement in comparison with the cup anemometer. It is technical details are shown below on *Table 5*.

Figure 22 FINO 1 ultrasonic anemometer

(Bundesamt für Seeschifffahrt und Hydrographie, 2018).

Table 5 FINO 1 ultrasonic anemometer specifications

(Bundesamt für Seeschifffahrt und Hydrographie, 2018).

FINO1 ultrasonic anemometer technical specifications	
Manufacturer	Gill Instruments R3-50
Measurement range	0-45 m/s
Resolution	0.01 m/s and 1°
Measurement interval	50 Hz
Logging interval	10 Hz
Height	Orientation to boom from the mast
81,5 m LAT	311°
61,5 m LAT	308°
41,5 m LAT	308°

The cup anemometers cover all the height in consideration (30-100 m) with orientation around 140º and can be considered as Southeast (SE) direction, whilst the ultrasonic anemometers cover the heights 40, 60 and 80 m with orientation around 310º and can be considered as North-West (NW) direction. This information is relevant since the wind data will be selected according to the wind direction to make sure that the processed data has no mast disturbance effect.

Wind vane measures the wind direction of horizontal wind speed, and its technical specifications are presented below on *Table 6.* In order to give the resulting wind direction, deflection of the wind vane axis by the wind is transferred to a circular potentiometer.

Table 6 FINO 1 wind vane specifications

(Bundesamt für Seeschifffahrt und Hydrographie, 2018).

FINO1 wind vane technical specifications	
Manufacturer	Adolf Thies GmbH & Co.KG
Threshold	0,5 m/s
Measurement interval	1 Hz
Logging interval	1 min
Height	**Orientation on boom off mast**
91,5 m LAT	315°
71,5 m LAT	307°
51,5 m LAT	310°
34m LAT	307°

Fourteen years of observation data from January 2004 to January 2018 taken from the official BSH database website (*http://fino.bsh.de*), originally in the format of '.dat'. is filtered and utilized in this study.

4.1.1.1 Data Filtering

The long term FINO 1 data set used in this study is 14 years of data at a 10-minute interval, starting from January 01st, 2006 to October 01st, 2018 with possible data return of 771,402 records.

Through additional top anemometer installed at a 104.5 m LAT height, Westerhellweg et al., 2012 presented the ratio of the wind speeds of this additional anemometer and the top anemometer at 103 m, resulting a flow distortion of the booms at wind directions 0°, 90°, 180°, and 270°. Westerhellweg et al. (2012) displayed the mast correction and its uncertainty, showing that for FINO 1, the cup anemometers had the highest mast correction in the range of wind direction 300° to 360° while for sonic anemometers, the highest mast correction was in the range of wind direction 100° to 150°. Wind shear and stability effects were also the causes for the uncertainty of the mast correction.

For the analyses, the wind data measurements were selected based on the undisturbed wind direction. FINO1 has two side of masts sitting on different booms in two opposite directions, leaving a valid measured zone for each instrument, as illustrated in *Figure 23*. As mentioned in ***Section 4.1.1***, from the ultrasonic anemometer data (boom direction around 310°) will be extracted the wind direction 240° to 30° and the wind direction 30° to 240° will be extracted from cup anemometer data (boom direction around 140°).
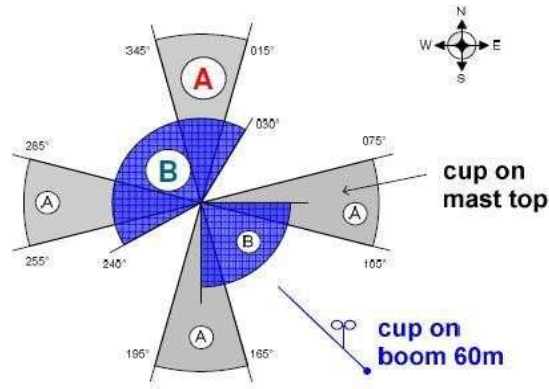
Figure 23 Arrangement of FINO1 instruments placement (wind vane, cup, and ultrasonic anemometer).

Since our focus is on power production, time periods with turbine fault codes, known here as NaN values were filtered out, ~50.9% less data. The codes filtered out were possible related to grid loss, maintenance, repairs, stops, wind direction curtailments or bad data that were not classified further. A total of 379,026 records for each of the seven elevations (from 40 to 100m) were available. Finally, values of $\overline{U}_{ref}$ higher than $\overline{U}(z)$ were removed, to have a representative shear exponent (shown in **Section 3.1.1**). After filtering data, a total of 282,719 records remained, representing ~36.65% of original data.

A wind rose *Figure 24* with wind speed at 80 m was selected at FINO 1 only to present the dominant wind direction. Additionally, this altitude allows us to select measurements on either side of the mast and avoid distortion effects. Wind direction data at 90 m was used as this was deemed to be the most reliable measurement of wind direction (Kettle, 2013).
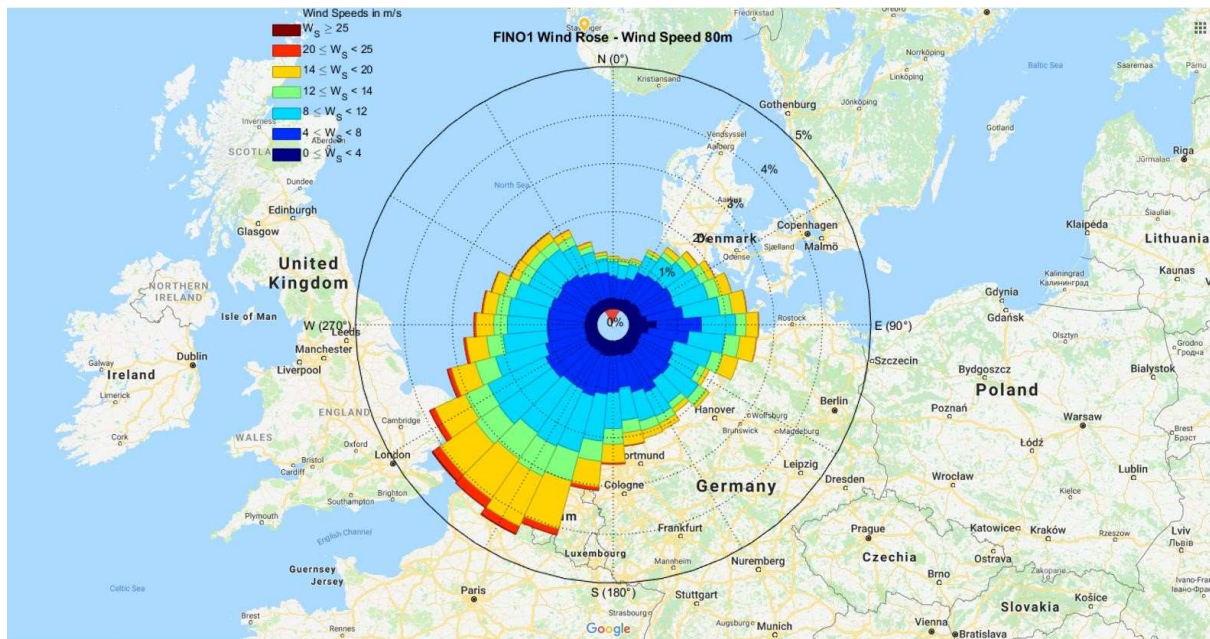
Figure 24 Wind rose of data return for the wind speed observations at 80 m heights at FINO1 from January 01st, 2006 to October 01st, 2018; alongside google map presentation of FINO 1 location at the North Sea

As can be seen above, high wind speeds were coming from the English Channel between France and UK as well as from Belgium side with the highest wind speeds captured from this South-West (SW) direction in the range of 20 to 25 m/s. Most frequent wind speeds are in the range of 10 to 15 m/s. The wind speeds distribution in the research platform FINO 1 is consistent with the prediction, with South-West direction near lands having higher frequency of high wind speeds due to the land breeze – when winds blow from higher pressure over the land to lower pressure over the sea (Ackerman, 1995). Winds coming from the North-West (NW) and East direction are the second most frequent ones with maximum wind speeds between 15 and 20 m/s.

4.1.2 Dataset – FINO 3

The wind data comes from a 120 m high Forschungsplattform in Nord-und Ostsee 3 (FINO3) offshore research platform. It is located about 80 km west off the coast of the German North Sea island of Sylt (55° 11,7 'N, 007° 9,5' E), in the midst of German offshore wind farms (Butendiek, DanTysk, Sandbank and Nördlicher Grund), being operated since August 2009.

The met mast has a platform at 22 m height and wind speed is measured at several elevations from 30 m to 100 m *Figure 25a*. The research platform FINO 3 can also provide other meteorological measurements such as wind direction, air temperature, moisture, air pressure, global radiation, relative humidity, and precipitation *Figure 25b*. More info found at *http://www.FINO3.de* page.

Figure 25 FINO3 met mast design and measurement heights.

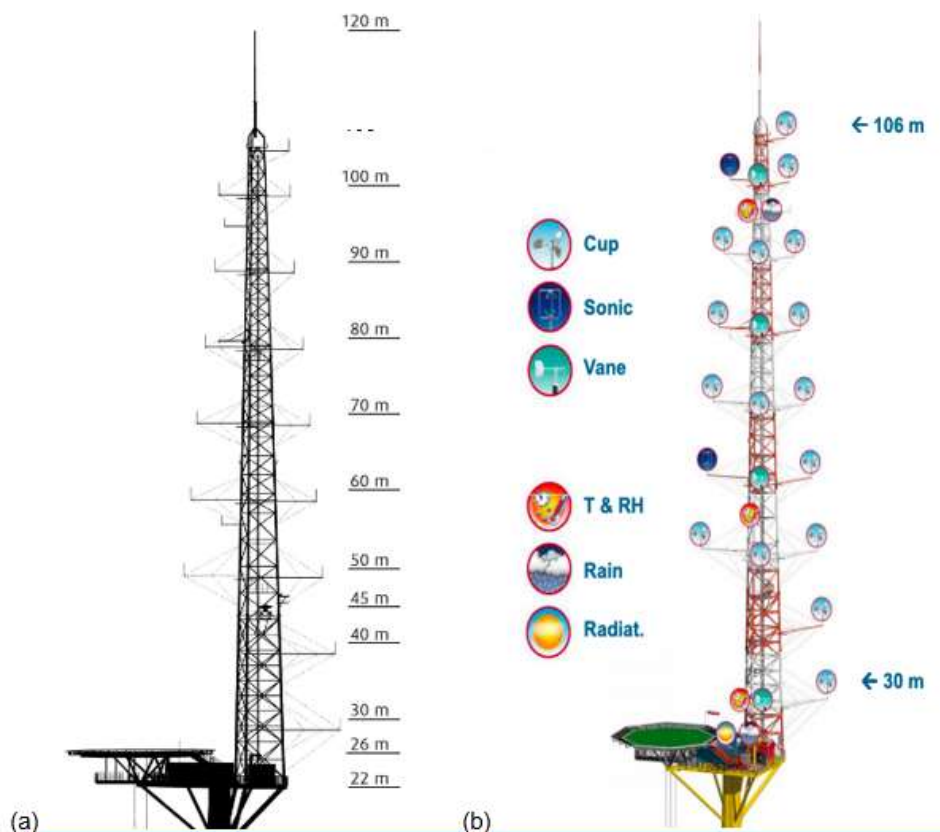The platform has a triangular cross-section (2.63 m side) with one, two or three booms at different height levels in order to minimize mast distortion effects. The three booms orientations are shown in *Figure 26* (225°, 345° and s105°, named respectively A, B and C from here on). This layout configuration allows the selection of wind sectors undisturbed by the mast.
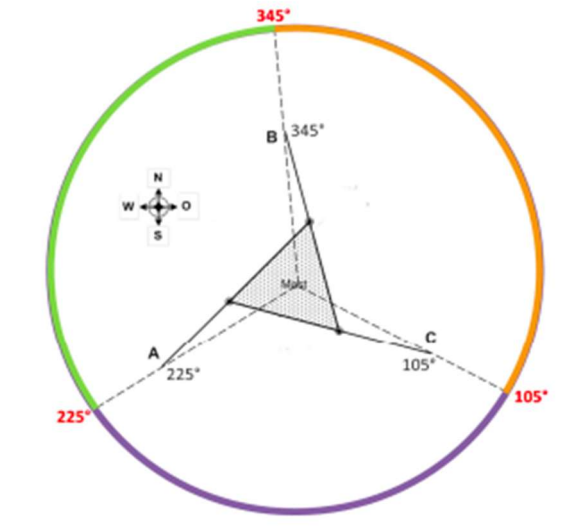
Figure 26 Orientation of the three booms at the FINO3 platform.

Another instrument available is wave buoy which records significant wave parameters (wave height, wave direction, up crossing period and wave peak period).

Nine years of observation data, from September 2009 to August 2018, were taken from the official BSH database website, *http://fino.bsh.de*, originally in the format of '.dat'. is filtered and utilized in this study.

4.1.2.1 Data Filtering

Wind measurements are heavily affected when the corresponding sensor is located in the wake of the mast tower. M. C. Holtslag et al. (2015) could show that when the sensors were located directly behind ($\mp$ 10º) the tower structure, it experienced significantly reduced wind speeds and when one sensor was located directly in front of the tower, both remaining sensors located more to the side of the tower experienced increased wind speeds while the sensor in the front of the tower experienced a reduced wind speed. The tower structure presence causes locally a weak increment in wind speed sideways of the tower and a significant reduction of wind speed behind the tower. Therefore, it is decided to determine the actual wind speed at different heights based on the wind direction and filter wind speed measurement from booms in wind sectors that has no mast disturbance.

The possible wind directions were divided into six sectors as shown below in *Figure 27a*. An assumption was made with regards to the selection of the wind speed measurement. For boom A, the wind speed measurements are undisturbed for wind direction in (105° to 165°) & (285° to 345°) sectors, boom B measurements are undisturbed for wind direction in (45° to 105°) & (225° to 285°) sectors and boom C measurements are undisturbed for wind direction

54

in (165° to 225°) & (345° to 45°) sectors (See *Figure 27b*). The wind direction at 100 m on boom C is used.
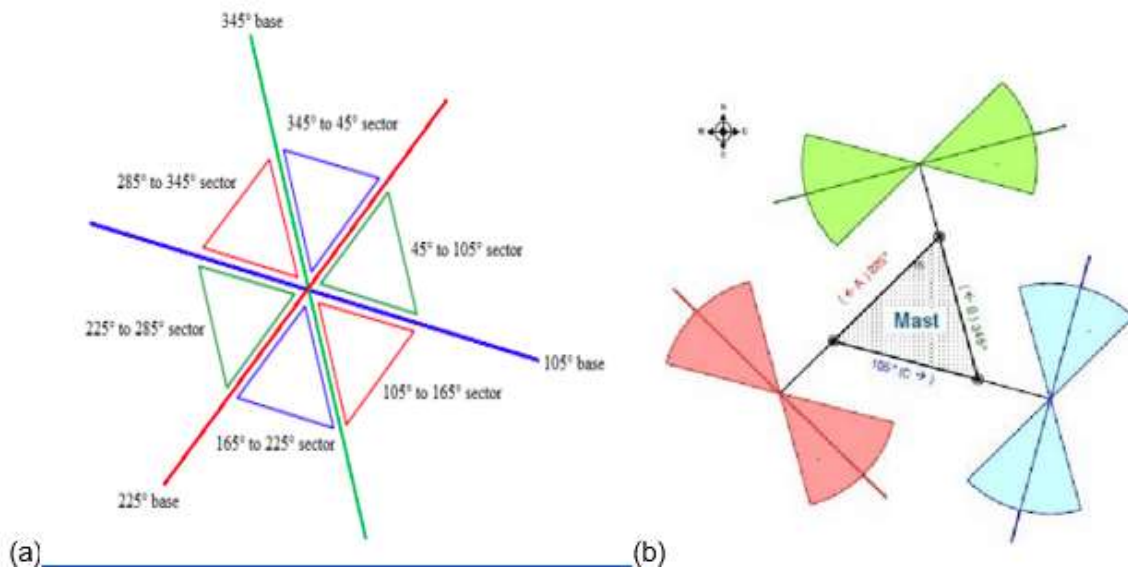
Figure 27 Wind direction at FINO3 divided into six sectors

(sectors are shown in (a) and the corresponding undisturbed sectors for each boom are shown in (b)).

A breakdown of the wind speed measurements data return at different heights from September 2009 to August 2018 based on this selection process is shown in *Table 7*. The possible data return for this period is 473,328 records of 10-minutes average wind speed for each of the nine heights, including the non-available measurements (known as NaN values due to technical problems).

Values of $\overline{U}_{ref}$ higher than $\overline{U}(z)$ were removed to have a representative shear exponent (shown in *Section 3.1.1*). Besides, NaN values were filtered out. After applying the filters outlined in this study, a total dataset of 291,446 observations remains for the period of September 2009 to August 2018, representing ~61.57% of original data set.

Table 7 Data return at the various measurement heights at FINO3 based on 9 years of data from September 2009 to August 2018 (The possible data return for this period is 473,328 records of 10-minutes average values)

Elevation (m)	Boom A (105° to 165°) & (285° to 345°) sectors	Boom B (45° to 105°) & (225° to 285°) sectors	Boom C (345° to 45°) & (345° to 45°) sectors	No of available data	% of possible data return
30	NO	YES	NO	160986	34.01%
40	NO	YES	NO	156467	33.06%
50	YES	YES	YES	431446	91.15%
60	YES	YES	NO	307896	65.05%
70	YES	YES	YES	434841	91.86%
80	YES	YES	NO	309479	65.38%
90	YES	YES	YES	411307	86.90%
100	YES	YES	NO	276674	58.45%
106	NO	YES	NO	153893	32.51%

For this analyze, it was decided to use the heights at 50, 70 & 90m where 3 booms are available, giving more representative wind speed measurements. A wind rose of data return for the wind speed observations at 90 m height, the highest elevation with three boom present, was plotted and is presented in *Figure 28*, showing the dominant wind direction between 225° to 285°.
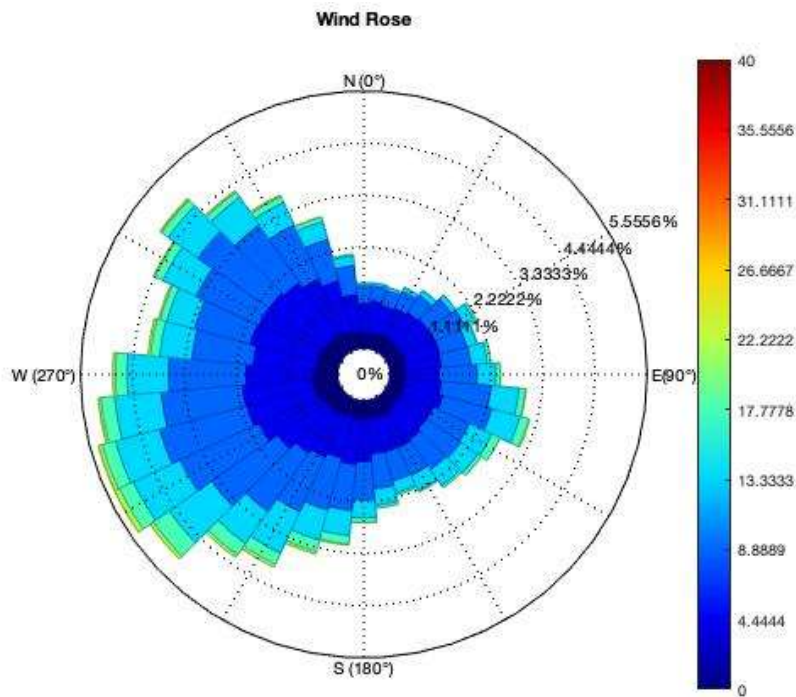
Figure 28 Wind rose of data return for the wind speed observations at 90 m heights at FINO3 based on 411,307 10-min mean wind speed observations from September 2009 to August 2018.

4.1.3 Dataset – Frøya

The Skipheia meteorological mast is operated by Norwegian University of Science and Technology (NTNU) and located at the western mid-Norway coast on the island of Frøya. The mast is located on land with geographical coordinates 8.34251 E and 63.66638 N, approximately 20 meters (above sea level) and with the shortest distance to the ocean being 300m in the south-southwestern direction. The site experiences winds coming in from the Norwegian Sea from the southwest, as well as onshore winds from the east.

The wind measurement station is containing three masts, as shown in *Figure 29*. Masts 2 and 4 are 100 meters high, whereas Mast 3 is 45 meters. The three masts are positioned relative to each other, showing intermediate distances and orientations *Figure 30*. Both 100-meter masts are equipped with ultrasonic anemometers, but in the present study, Mast 2 is the only one being considered.
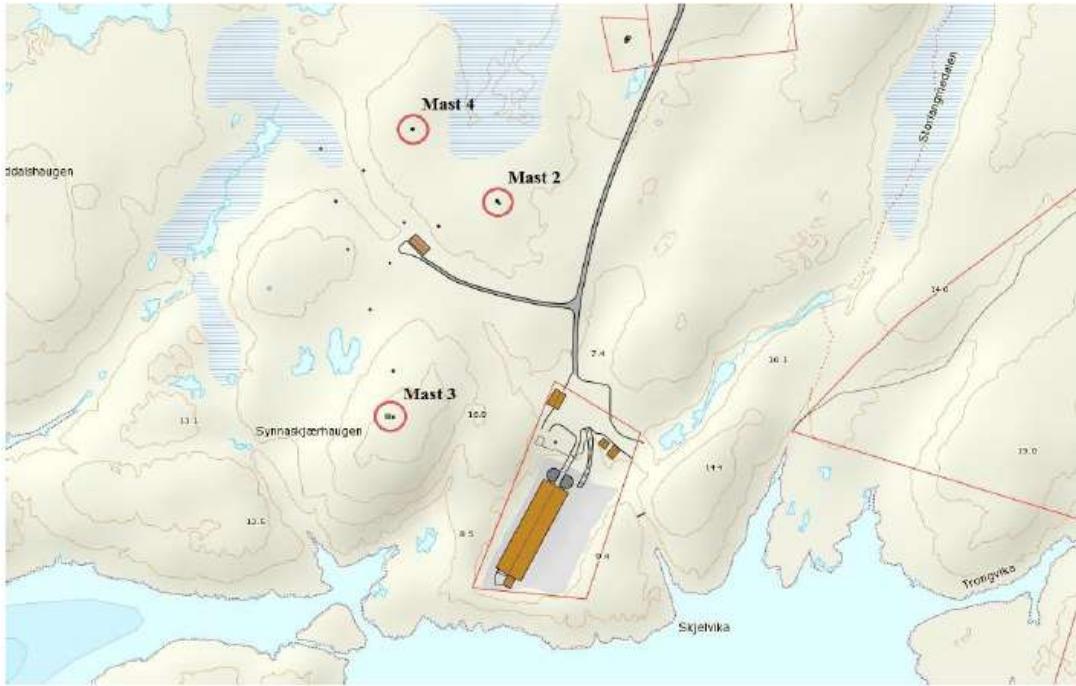
Figure 29 Map with contour lines and mast positions (Øistad, 2014)
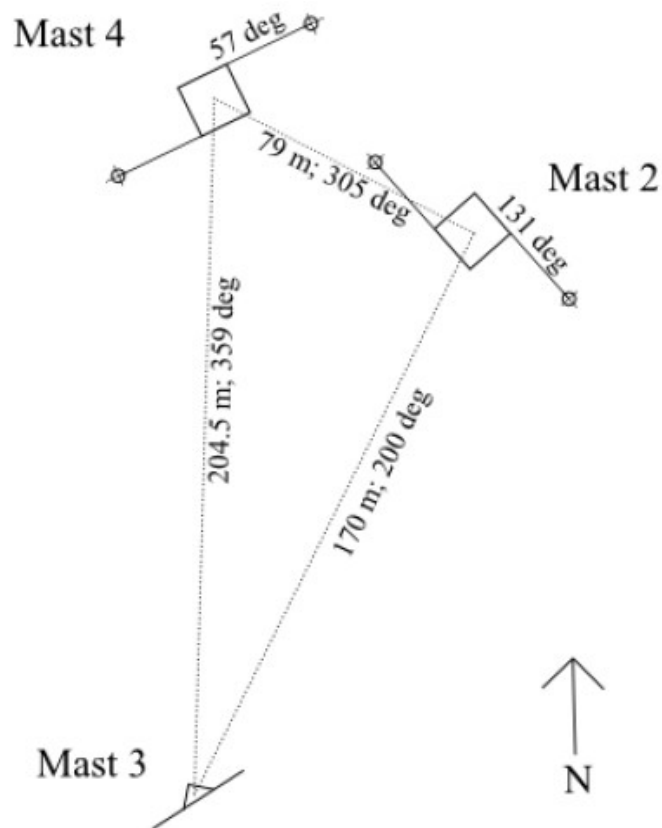
Figure 30 Mast positions and orientations (Øistad, 2014)

The site has six pairs of Gill WindObserver II 2D ultrasonic anemometers installed on the mast all together, at heights of 10, 16, 25, 40, 70 and 100 meters, respectively. Additionally, one Campell Scientific 109 temperature probe is mounted at each height, as well as at two meters above ground level near the mast. A Lambrecht rain sensor is used to measure the precipitation, and a Campbell Scientific CR3000 Micrologger is logging the data (Øistad, 2014). The site does not record pressure or humidity.

Table 8 shows an overview of the ultrasonic anemometers installed on the mast, "Geographical orientation" gives the orientation of the anemometer booms relative to the geographical north (i.e. 0°), and "Southeast" and "Northwest" mean 131° and 311°, respectively. The orientation of the booms can also be seen in *Figure 31*. The serial numbers of the respective anemometers are not known. (Øistad, 2014)

Table 8 Anemometer properties (Øistad, 2014)

Short name	Geographical orientation	Logger channel	Height above ground [m]
UA1	Southeast	1	10
UA2	Northwest	2	10
UA3	Southeast	3	16
UA4	Northwest	4	16
UA5	Southeast	5	25
UA6	Northwest	6	25
UA7	Southeast	7	40
UA8	Northwest	8	40
UA9	Southeast	9	70
UA10	Northwest	10	70
UA11	Southeast	11	100
UA12	Northwest	12	100

The anemometers are mounted on square-cross-sectional booms reaching 2.5 meters out from the tower, which has a quadratic climbable lattice shape and a ground surface area of 1 m2. A sketch of the mast including principle dimensions of the tower and the instrument mounting fixtures can be seen in *Figure 31*. Additionally, to the orientation of the booms, there is a displacement between the geographic north and the anemometer north of 221°. The red arrows in *Figure 31* show the northerly directions on the anemometers, pointing southwest (221°) and northeast (41°), respectively. A summary of the measurement features of the mast is given in *Table 9.* (Øistad, 2014)

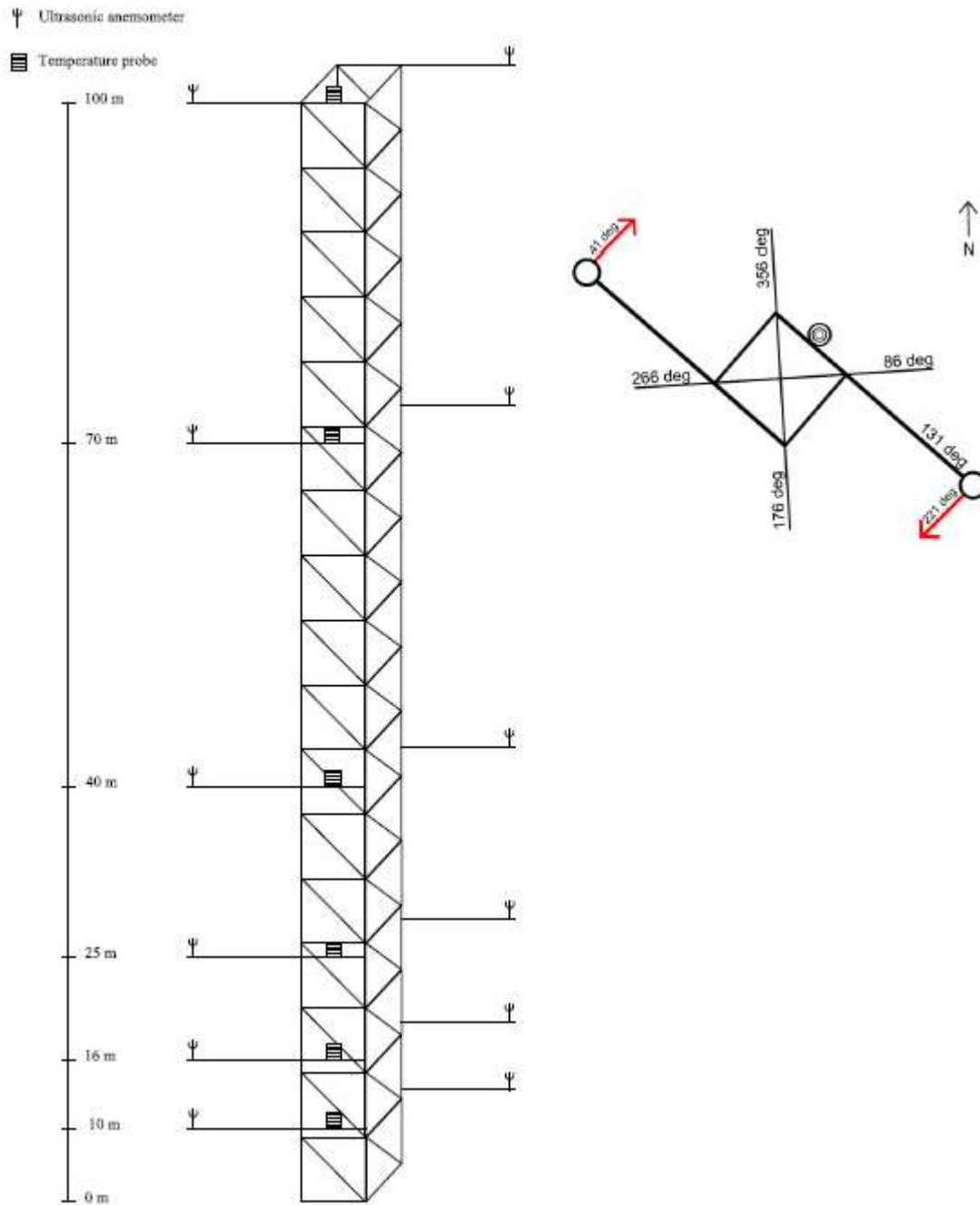*Figure 31* Left: Sketch of Mast 2 with anemometers and temperature sensors

Right: Top view of mast showing anemometers, temperature sensor and directions

Table 9 Mast features (Øistad, 2014)

Mast features - Mast 2 Skipheia	
Mast coordinates	63.66638N, 8.34251E Altitude: 20 meters above sea level
Time period with available data	2009-11-18 - 2015-01-01
Sensors types	Gill WindObserver II ultrasonic anenometers (12 pcs) Campbell Scientific 109 temperature probe (7pcs)
Data logging system	Data logger: Campbell Scientific CR3000 Micrologger Averaging period: 10 minutes Sampling rate: 1Hz
Mast type	Climbable lattice tower (1x1 m2), 100 meters

4.1.3.1 Data Filtering

The wind data return being assessed here are from November 2009 to January 2015 with possible data return of 269,197 records of 10-minutes average wind speed for each of the heights (from 10 to 100 m height) at Shipheia. The measured data from the mast were provided as mat files (MATLAB) containing ten-minute averaged measurements for wind speed, wind direction, air temperature, standard deviations for speed and direction, and availability for the anemometers. Signals are sent from the measurement instruments to the data logger with a sampling rate of 1 Hz, and from the data logger to a computer running the software LoggerNet 3.4.1, developed by Campell Scientific. For this study, only wind data at 40, 70 and 100 m heights are used due to the lower tip height for the reference wind turbine in this study being at 30 m.

The mast has two anemometers at each respective height, hence the need to combine the anemometer data. They are mounted with an orientation difference of 180° and will hence perceive mismatching wind parameters due to mast shading. *Figure 32* shows the ratio of the wind speed sensors as a function of wind direction. The three heights were analyzed separately. A peak can be observed at approximately between 105º – 140º and a dip at approximately between 335º – 285º. The plot in *Figure 32* corresponds to the expected tower distortion effect on the anemometers, caused by wind shading. To handle this, a MATLAB code was used to combine the data from the two respective anemometers for each of the three elevations in each time step, choosing the one not disrupted by the tower. After combining the measurements for the 6 anemometers (two in each height), the data set contained one value for wind speed and one for wind direction at each height in every time step.

Since our focus is on power production, time periods with turbine fault codes, known here as NaN values, were removed. A breakdown of the wind speed measurements data return at the three heights from the given period based on this selection process is shown in *Table 10*. In addition, $\overline{U}_{r_{ef}}$ higher than $\overline{U}(z)$ values were removed, to have a representative shear exponent (shown in **Section 3.1.1**). A total of 95,119 records remain representing 35.33% of original data.
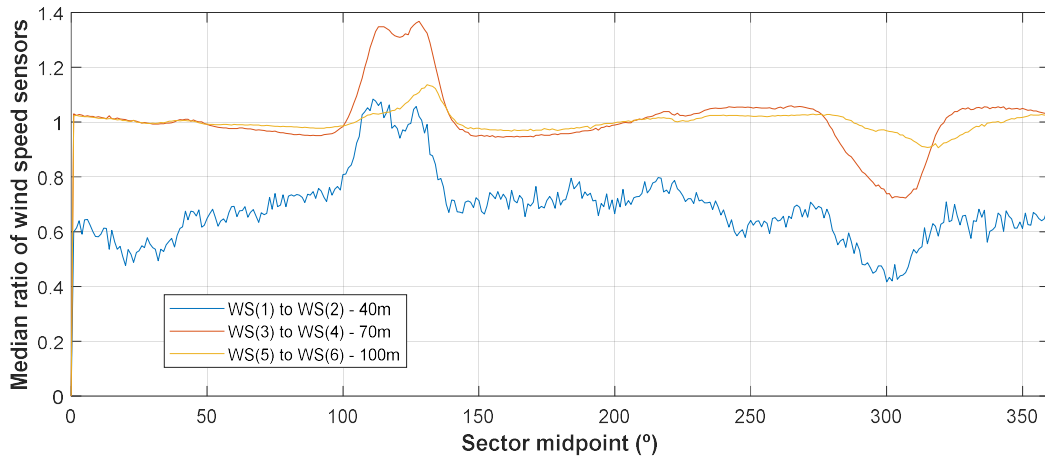
Figure 32 Wind speed ratio relative to wind direction

Table 10 Data return at the various measurement heights at Frøya based on 6 years of data November 2009 to January 2015 (The possible data return for this period is 269,197 records of 10-minutes average values)

Elevation (m)	Boom A (41° to 221°) sectors	Boom B (180º) sectors	Nº of available data (after selection process)	% of possible data return
40	YES	YES	119270	44.30%
70	YES	YES	118581	44.04%
100	YES	YES	118561	44.04%

A wind rose *Figure 33* for all heights for the given period was plotted to assess the wind direction detected by the mast to distinguish the measured parameters as representative for onshore or offshore wind, as mentioned in **Section 4.1.3**.
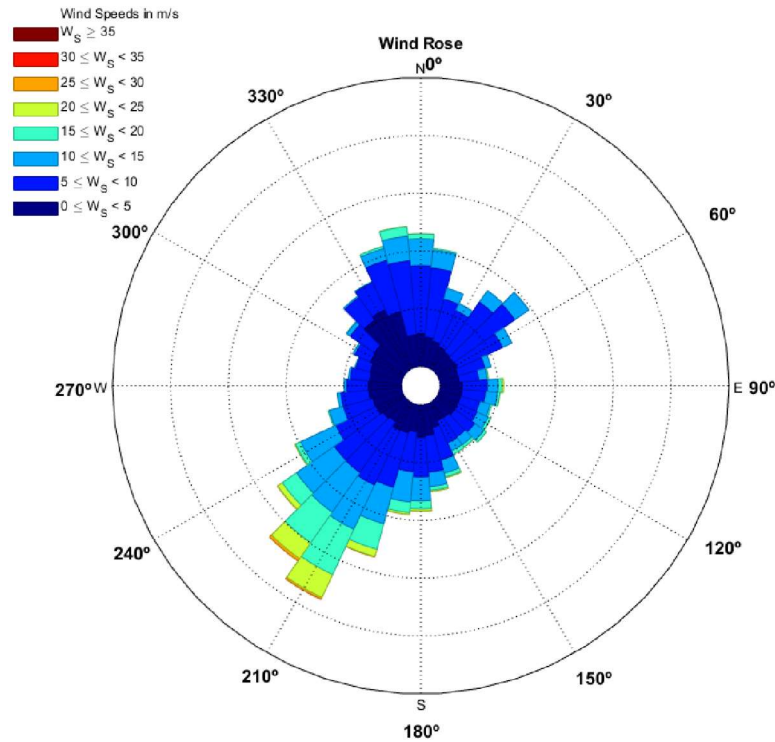
Figure 33 Wind rose showing the direction frequency for all heights

It can be seen in the plot above that the sector with midpoint 210° (i.e. winds from southwest), represent the bulk of the wind direction distribution. Another notable orientation is northwest. The southwest frequency bulk implies winds from the Norwegian Sea. From approximately 235° via north to 50°, the west end of Frøya is exposed to nearly undisturbed maritime winds (Heggem et al. 1997), which implies that these measurements are representative for offshore conditions. An overview describing the various directions is given in *Table 11*.

Table 11 Classification of wind direction sectors (Heggem et al. 1997)

Direction	Description
0°-40°	The distance to the sea is 3-5 km
40°-100°	Wind that has passed the northeast part of Frøya for up to 25 km
100°-190°	Wind comes from inland, but have passed sea for the last 10 km
190°-270°	The sector with the most frequent wind direction and the highest average wind speeds. The distance to the sea varies from 300 m to 3 km
270°-360°	Maritime wind that have passed land for about 3 km

5. Comparison between Power Law and Logarithmic Law Profiles

For this study, it was decided to access the performance of power law and standard logarithmic law profiles to estimate wind speeds for different elevations. A comparison between the estimated wind speed results of the two models against the measured wind speed data was carried out in order to identify a suitable model that could represent offshore wind profile, and allow to extrapolate for the various heights up to tip height of 208 m, that can be used to estimate power generation.

With the filtered average measured wind speed data for different heights, the new wind speeds were estimated according to **Section 3.1.1** for the power law model. A wind shear coefficient was estimated as recommended by Wilfried et al. (2019), to assess the new wind speeds for various heights above measurement points. Due to extensive shear exponent estimated data for the period given in each of the three different locations, they are not shown here. For the logarithmic model, the *equation 12* below was used, another approach to obtain wind speed using two different heights and a known terrain roughness, 0.003. Furthermore, a comparison was done between the average measured wind speed and the normalized average estimated wind speeds obtained from the two wind profile models. The performance of the wind profiles was then assessed, and the analysis & results of the assessments can be seen in *Figure 34* & *Figure 35*. Both calculations were done for the three different locations considering the filtered data for their specific period given.

The logarithmic wind profile is given as:

$$\frac{\overline{U}_{z1}}{\overline{U}_{z2}} = ln(\frac{z_1}{z_0})/\ ln(\frac{z_2}{z_0}) \qquad [12]$$

$\overline{U}_{z_1}$ — is the known wind speed (m/s) at height z_1;
$\overline{U}_{z_2}$ — is the wind speed (m/s) to be calculated at height z_2;
z_1 — is the reference height (m) where $\overline{U}_{z_1}$ is known;
z_2 — is the height (m) above ground level for $\overline{U}_{z_2}$;
z_0 — is the aerodynamic roughness length (m).

Finally, the RMSE (root mean square error) at the different heights for each wind profile model stated above was evaluated to understand the magnitude of the over/underestimation of the wind speeds at the various observation heights, as seen in *Figure 36, Figure 37* & *Figure 38*. The RMSE between the estimated wind speed $\hat{u}_i$ by the wind profile models and measured wind speed u_i is given as:

$$RMSE\ =\ \sqrt{\frac{\sum_{i=1}^{n}\ (\hat{u}_i - u_i)^2}{n}} \qquad [13]$$
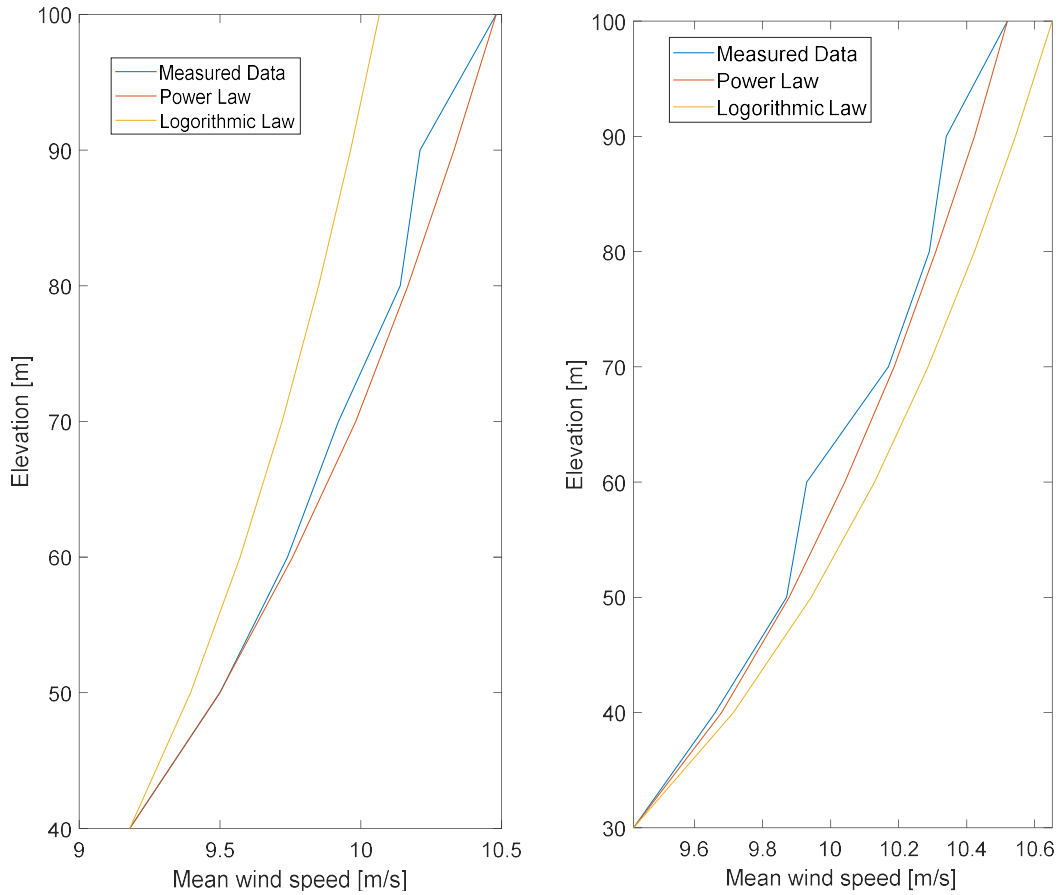
Figure 34 All filtered data (The normalized average wind speed of the measured wind speeds and the wind profile models for FINO 1 and FINO 3, respectively).
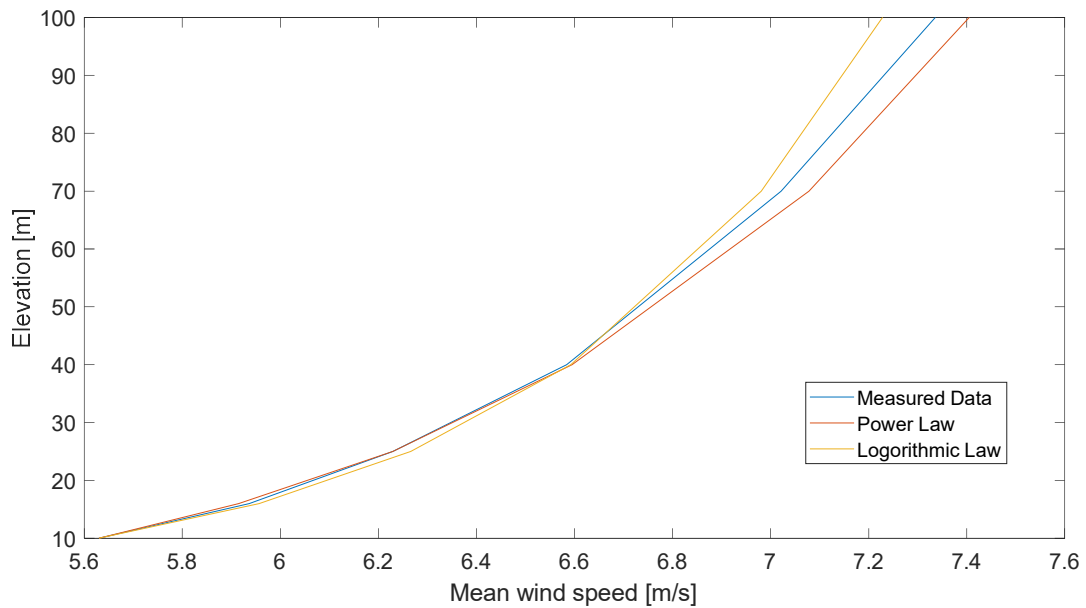
Figure 35 All filtered data (The normalized average wind speed of the measured wind speeds and the wind profile models for Frøya.

For FINO 1, the power law profile corresponds well to the observations up to circa 60 m height as seen in *Figure 34.* Beyond that elevation, the wind speed was overestimated with maximum RMSE of 0.0145m/s as shown in *Figure 36*. The logarithmic profile underestimated the wind speed for all observation heights. The magnitude of the underestimation increased gradually with increasing elevation, with an exception at 90 m height, with maximum RMSE of approximately 0.05m/s. The RMSEs of the power law profile were lower for all observation heights compared to the RMSEs of the logarithmic one as shown in *Figure 36*.

For FINO 3, both profile models overestimated the wind speed for all observation heights with a better performance of power law profile as seen in *Figure 34* with maximum RMSE of 0.0125m/s shown in *Figure 37*. Again, the RMSEs of the power law profile were lower for all observation heights compared to the RMSEs of the logarithmic one as shown in *Figure 37.*

For Frøya, the power law underestimated the wind speed up to approximately 25 m height where it started to overestimate the wind speed until 100 m height with maximum RMSE of 0.0111m/s as seen in *Figure 38*. The logarithmic profile overestimated the wind speed up to approximately 40 m height where started to underestimate the wind speed until 100 m with maximum RMSE of 0.0174m/s as seen in *Figure 38*.

	50m	60m	70m	80m	90m	100m
Log	0.0127	0.0204	0.0242	0.0352	0.0299	0.0503
Power	0.0001	0.0022	0.0074	0.0033	0.0145	0

Figure 36 RMSE at the various heights of the wind profile model for FINO 1

	40m	50m	60m	70m	80m	90m	100m
Log	0.006	0.008	0.0221	0.0129	0.0148	0.0226	0.0146
Power	0.0022	0.0009	0.0125	0.0018	0.0021	0.0093	0
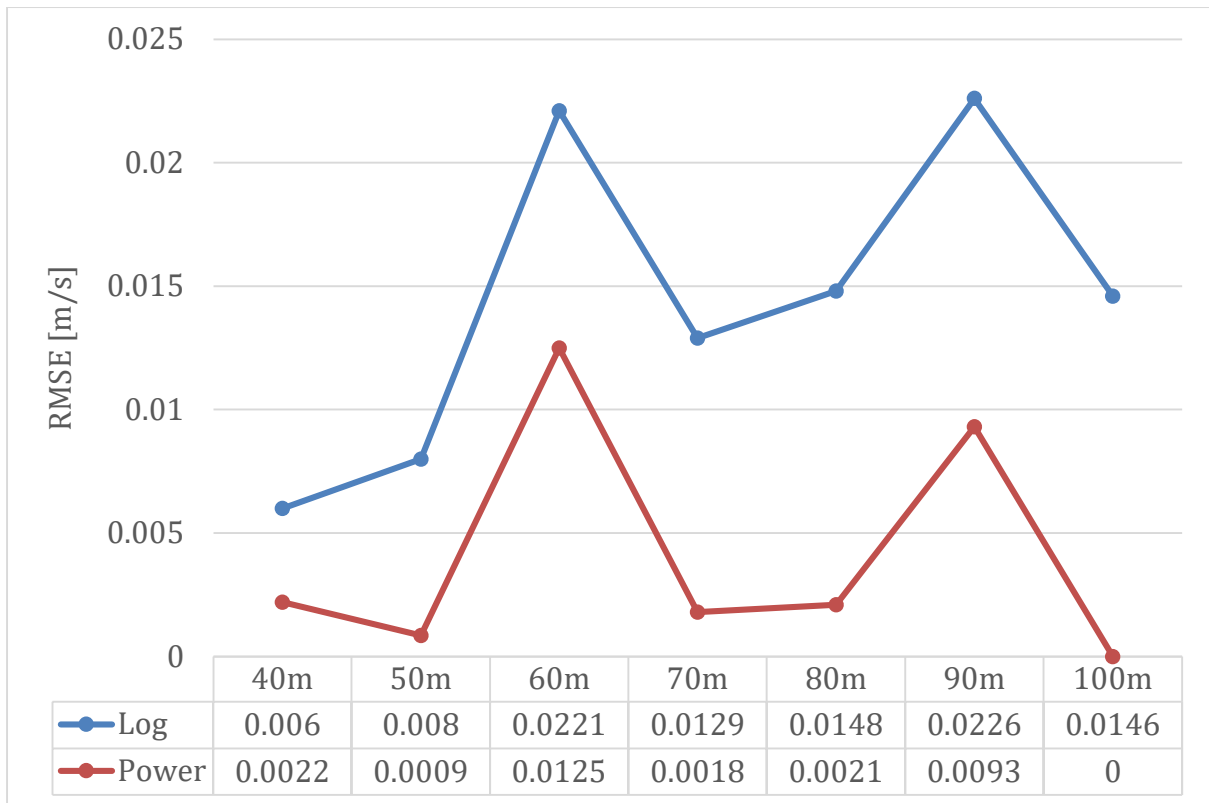
Figure 37 RMSE at the various heights of the wind profile model for FINO 3

	16m	25m	40m	70m	100m
Log	0.0033	0.0059	0.0013	0.0065	0.0174
Power	0.0034	0.0000	0.0018	0.0092	0.0111
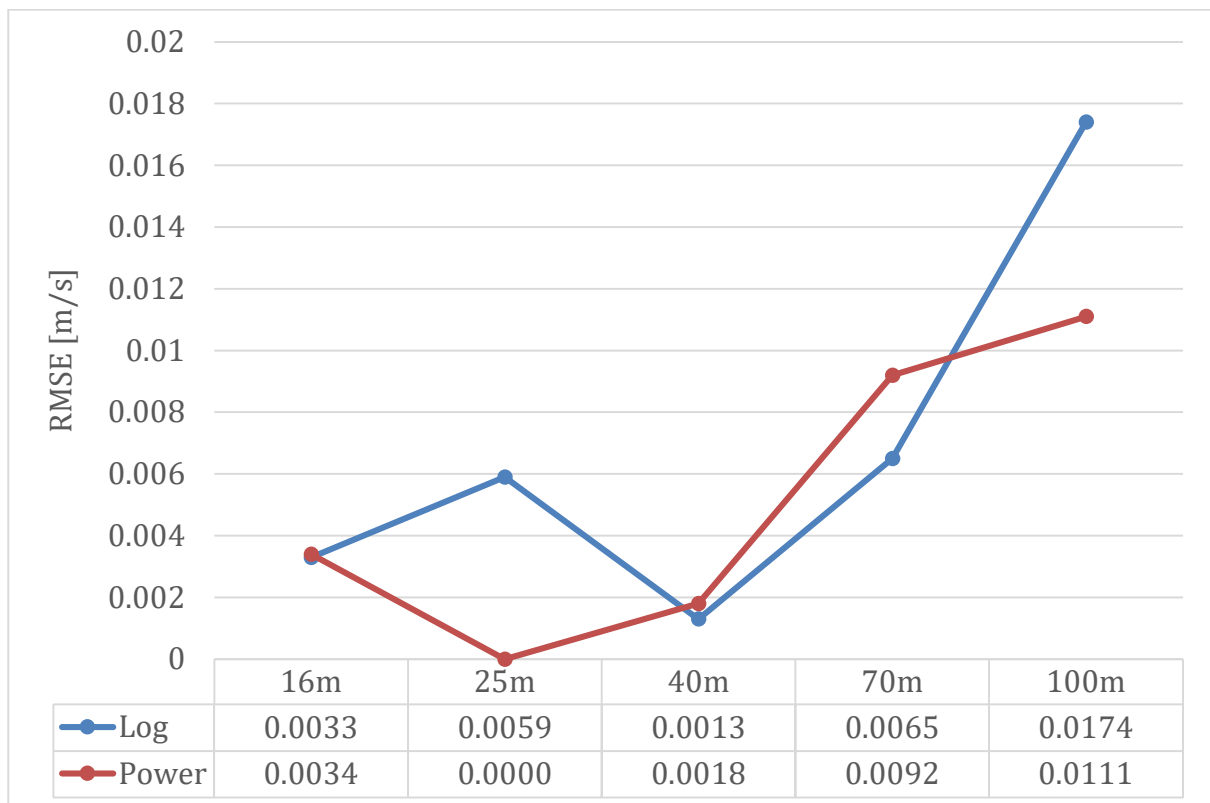
Figure 38 RMSE at the various heights of the wind profile model for Frøya

6. Power Curve, Wind Profiles Analysis and Results

6.1 Power Curve

DTU 10-MW Reference wind turbine (Bak, C. et al. 2013) power curve was assumed as input for the base case in this research. *Table 12* gives the design summary of the DTU 10 MW wind turbine and *Figure 399* shows the power curve used.

Table 12 DTU 10-MW Reference Wind Turbine Design Summary

Characteristic	Value
Rating	10MW
Rotor orientation, configuration	Upwind, 3blades
Control	Variable speed, collective pitch
Drivetrain	Medium speed, Multiple stage gearbox
Rotor, Hub diameter	178.3m, 5.6m
Hub height	119m
Cut-in, Rated, Cut-out wind speed	4m/s, 11.4m/s, 25m/s
Cut-in, Rated rotor speed	6RPM, 9.6RPM
Rated tip speed	90m/s
Overhang, Shaft tilt, Pre-cone	7.07m, 5º, 2.5º
Pre-bend	3m
Rotor mass	229tons (each blade ~41tons)
Nacelle mass	446tons
Tower mass	605tons

The cut-in and cut-out speeds are the operating limits of the turbine. By staying in this range, you ensure that the available energy is above the minimum threshold and structural health is maintained. The rated power, a point provided by the manufacturer, takes both energy and cost into consideration. Also, the rated wind speed is chosen because speeds above this point are rare. Typically, one can assume that a turbine design that extracts the bulk of energy above the rated wind speed is not cost-effective.
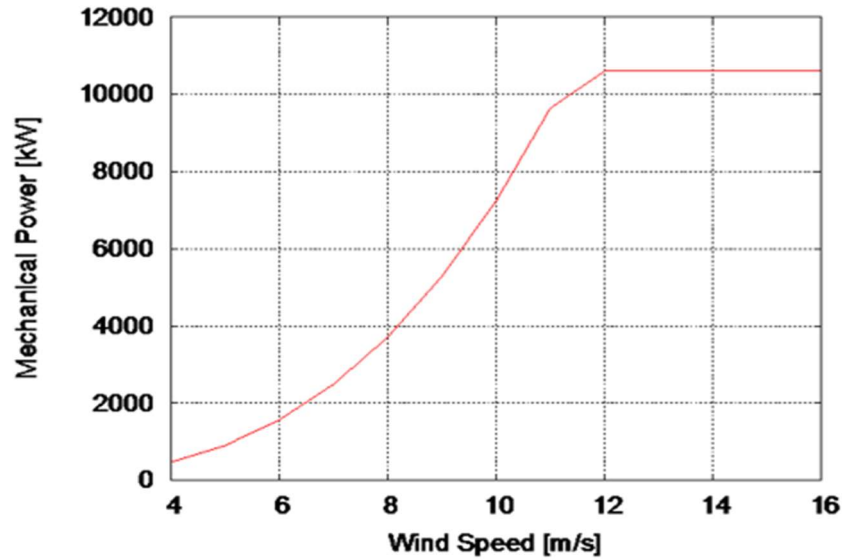
Figure 39 The power curve of the DTU 10 MW reference wind turbine (Bak, C. et al. 2013).
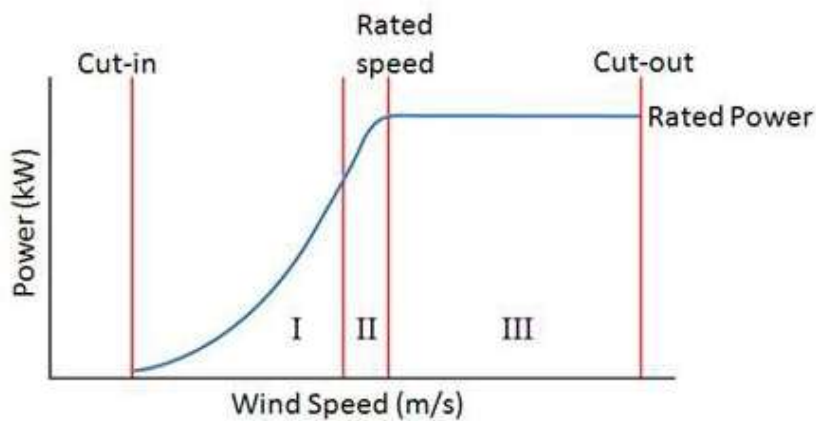
Figure 40 Ideal Wind Turbine Power Curve (Source: ni.com)

From *Figure 40*, the power curve is split into three distinct regions. Because Region I consists of low wind speeds and is below the rated turbine power, the turbine is run at the maximum efficiency to extract all power. In other words, the turbine controls with optimization in mind. On the other hand, Region III consists of high wind speeds and is at the rated turbine power. The turbine then controls with limitation of the generated power in mind when operating in this region. Finally, Region II is a transition region mainly concerned with keeping rotor torque and noise low.

6.2. Wind Profile Extrapolation Analysis and Results – Power Law

Further calculations will be based on the power law profile since it showed to be better performing model to extrapolate wind speeds for different elevations as illustrated in **Section 5**. To cover the rotor cross-section area of a 10-MW WTG with assumed lower and upper tip heights at 30m and 208m, respectively, the rotor area was divided into segments. An extrapolation of the wind speed was done for different elevations, from 110m up to the upper tip height, for all the three scenarios. The wind data was fitted to a power law profile to get a wind shear exponent, alpha factor (α) presented in **Section 3.1.1**, to be able to estimate the vertical wind speed profile. The -999 values were filtered out from the data to eliminate the complex double numbers in the shear exponent calculation. In addition, to have a representative shear exponent, data was filtered in a way that $\bar{U}(z)$ would always be higher than $\bar{U}_{r_{ef}}$. Once the new heights and wind speed data were defined, the REWS method, presented in **Section 3.6.2**, was calculated according to *IEC 61400-12-1* standard, assuming a hub height of 119m and a rotor diameter of 178m as stated in *Table 12*. The wind speeds at hub height were also calculated based on the estimated alpha factor.

The following step was to correlate equivalent wind speed to a 10-MW power curve, as shown in *Figure 39*. Zero values were given to wind speeds with values below cut-in speed, 4m/s, and above cut-out speed, 25m/s. Then, the corresponding power output was obtained for the equivalent wind speed and hub height methods between cut-in and rated speeds, 4 & 11.4 m/s, respectively, from the power curve.

Wind speeds were extrapolated to account for the kinetic energy flux through the swept rotor area of a 10-MW offshore reference wind turbine with tip height of 208m. Additionally, to reduce the discrepancies in the results that would not be related to the REWS model, there was no correction of the data for air density, required in the *IEC standard*. When applying the REWS method, in theory, the wind speed measured at each height should be corrected for air density at the same height; however, this variation is small (*IEC 61400-12-1 standard*). The air density was assumed to be constant with height.

Finally, a summation of all the power produced with the REWS method and all the power produced with the HHWS, calculated according to **Section 3.6.1**, was generated for comparison as shown in *Table 13, Table 14* & *Table 15*.

The percentage difference is calculated as:

$$\% \, Difference = \frac{U_{Equivalent} - U\_HubHeight}{U\_HubHeight} \times 100 \qquad [11]$$

6.2.1 Wind Power Results using Power Law profile

Some considerations applied for the data are summarized as below:

Research platforms - FINO 1 and FINO 3

→ Wind data are in the direction of coming to the mast (direction of the instrument receiving data is towards the mast).

→ For FINO 1, the use of wind direction at 90 m as it was found to be the most complete data (Kettle, 2013).

→ Processed data for wind speeds at 40, 50, 60, 70, 80, 90 and 100m heights for FINO 1. For FINO 3, wind speeds at 50, 70, and 90 m heights where used since 3 booms are available at each of those heights given more representative data. The wind direction at 90m height was used for FINO 3 analyses.

→ Wind data measurements were selected for the analysis based on the undisturbed wind direction described in *Sections 4.1.1.1* and *4.1.2.1*.

Frøya site

→ Processed data for wind speeds at 40, 70 and 100m heights since lower tip speed is at 30m.

→ Wind data measurements were selected for the analysis based on the undisturbed wind direction described in *Sections 4.1.3.1*.

Results were acquired by fitting the wind speed measured filtered data at different heights to a power law function (as shown in *Section 3.1.1*) to extrapolate the wind speed at various elevations up to tip height. The heights in the profile are spatially distributed evenly, except for the one at hub height shown in *Table 16*. The REWS was then calculated according to *Section 3.6.2* and adapted the weighting to the profile, defining the limit between two consecutive segments as the middle height between two consecutive wind speed extrapolated heights, presented in *Table 16*, as required by the REWS method.

For all the research platforms, the REWS model results in higher estimate of the power production compared to the hub height wind speed concept, a difference of ~3.2 – 8.9% as seen in *Table 13, Table 14* & *Table 15*, showing that when comes to rotors of modern multi-megawatt wind turbines, a single-point measurement (HHWS) can result in inaccurate and potentially inconsistent prediction of the power production.

Table 13 Power production - FINO 1 site based on 14-years period. From hub height power curve and REWS models.

Methods	Power Production (GWh)
REWS	328.03
Hub height	312.10

Table 14 Power production – FINO 3 site based on 9-years period. From hub height power curve and REWS models.

Methods	Power Production (GWh)
REWS	332.80
Hub height	322.23

Table 15 Power production – Frøya site based on 6-years period. From hub height power curve and REWS models

Methods	Power Production (GWh)
REWS	82.80
Hub height	75.44

Table 16 Details of profile and weighting function for FINO 1, FINO 3 & Frøya

Extrapolated Heights [m]	Segment weighting* (%)	Segment inferior limit height (m)	Segment superior limit height (m)	Segment height (m)
199	3.09	194	204	10
189	4.4	184	194	10
179	5.27	174	184	10
169	5.91	164	174	10
159	6.38	154	164	10
149	6.73	144	154	10
139	6.97	134	144	10
129	7.1	124	134	10
119	6.43	115	124	9
110	7.11	105	115	10
100	6.98	95	105	10
90	6.76	85	95	10
80	6.42	75	85	10
70	5.96	65	75	10
60	5.35	55	65	10
50	4.5	45	55	10
40	3.25	35	45	10
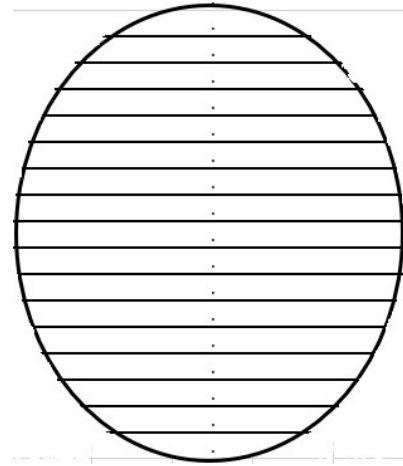
*ratio between the segment area (Ai in **Section 3.6.2**) and the rotor swept area (A in **Section 3.6.2**)

Note: Due to extensive data for the research platforms, the REWS values are not shown here.

7 Conclusion

This study compares the estimated power output for three sites from two different methods: rotor equivalent wind speed (REWS) versus wind speed at hub height (HHWS). For the simulation, wind speeds at different elevation, including at hub height, had to be extrapolated to cover the entire rotor disk. The power law and the logarithmic wind profiles were assessed as presented in *Section 5* in order to define a suitable wind profile that could represent offshore wind conditions. In overall, the power law profile outperformed the logarithmic law as extrapolation method to approximate average wind profile shape/shear conditions. The performance can be seen by making the comparison between the wind speed for the observation heights with the extrapolated data, as shown below.

For FINO 1, the power law profile corresponded very well to the observations up to circa 60 m height where started to overestimate with maximum RMSE of 0.0145m/s as shown in *Figure 36*. The logarithmic profile underestimated the wind speed for all observation heights. The RMSEs of the power law profile were lower for all observation heights compared to the RMSEs of the logarithmic one as shown in *Figure 36.*

For FINO 3, both profile models overestimated the wind speed for all observation heights with a better performance of power law profile as seen in *Figure 34* with maximum RMSE of 0.0125m/s shown in *Figure 37*. Again, the RMSEs of the power law profile were lower for all observation heights compared to the RMSEs of the logarithmic one as shown in *Figure 37.*

For Frøya, the power law underestimated the wind speed up to approximately 25 m height where it started to overestimate the wind speed until 100 m height with maximum RMSE of 0.0111m/s as seen in *Figure 38*. The logarithmic profile overestimated the wind speed up to approximately 40 m height where started to underestimate the wind speed until 100 m with maximum RMSE of 0.0174m/s as seen in *Figure 38*.

Based on the results here highlighted, power law was used to extrapolate wind speeds for various heights up to tip height at 208 m. For the three different offshore wind data sets with 14, 9 and 6-years of data respectively, a wind shear coefficient was estimated for each wind profile, as recommended by Wilfried et al. (2019), to estimate the new wind speeds for various heights above measurement points. Finally, comparisons are made between power production results obtained from HHWS and REWS methods as seen in *Section 6.2.1*.

In terms of available power estimates, for the three cases, results are consistent demonstrating that for a modern multi-megawatt wind turbines ignoring rotor-layer wind shear using a hub-height only estimate technique may lead to a significant underestimation of turbine available power. A difference of ~3.2 to 8.9% is observed as shown in *Table 13, Table 14 & Table 15*. The power estimate result follows Wilfried et al. (2019) expectations, presented in *Section 3.6.4*, when they concluded that the relevance of REWS approach is related to turbine dimensions, ie,the ratio of rotor diameter (D) and hub height (H). Although D/H was smaller than 1.8 in our study for the given 10-MW reference WT, the wind shear coefficient values were out of the range $-0.05 < \alpha < 0.4$ (not shown here due to extensive amount of data), highlighting the importance of REWS method.

In the past few years, as highlighted in **Section 3.6.4**, several studies related to wind speeds methods for power prediction were carried out by different authors showing different perspectives with some consensus as well.

Although this relation was not observed in this study, some researches have showed that the power estimation might vary based on location and vertical wind profile when using REWS and HH methods. R. Wagner, (2014) has concluded that the difference between the REWS and the wind speed at hub height depends on the site. In five cases, the REWS resulted in a higher AEP than the hub height power curve and in a lower AEP in two cases. Other studies showed that the REWS power curve can, depending on the wind shear profile, result in higher, equal, or lower AEP estimations compared to the AEP predicted by a HHWS power curve (F. Scheurich, 2016). Sperling et al. (2017) also concluded that the magnitude of the discrepancy between HHWS and REWS available power estimates varies by classified wind-profile type.

Since wind speeds had to be extrapolated, this may increase the uncertainty of the calculations and consequently in the power curve measurement. In an ideal situation, we would have a met mast that could cover tip heights of modern multi-megawatt wind turbines but since this is not feasible due to its implications related to construction, limiting it to maximum 100 m heigh, I recommend future research that compares REWS and HHWS results with observational data, using remote sensing devices (e.g. LIDAR) to better understand the implications of the results.

Based on our findings studying the power output by the turbine for the given periods for this three specific data sets, we concluded that the REWS will affect the estimate of the power production in a significant manner, especially if it takes into consideration the power output over the life cycle of the wind turbine, between 20-25 years. Due to some limitations on this research, a future work is proposed in the following section.

8 Future Work

This paper has presented a theoretical analysis to address the use of the rotor equivalent wind speed as advocated in the second edition of the *IEC 61400-12-1* standard since new, large wind turbines are being designed and installed. Wind speeds had to be extrapolated using a specific vertical wind profile since no observation data were available from 100 m up to tip height at 208 m.

IEC 61400-12-1 standard accounts for two different wind speed methods (HH & REWS) for power prediction. In addition, in this paper, at least three vertical wind profile types are presented in **Sections 3.1.1, 3.1.2 & 3.1.3** besides the ones mentioned in **Section 3.3**, machine-learning model and extended wind profile (Gryning's boundary layer shear profile). In the past few years, several studies related to both of those topics, wind speeds methods for power prediction and optimal wind speed extrapolation model were carried out by different authors showing different point of views with some consensus as well as highlighted in **Sections 3.3 & 3.6.4**.

To be in compliance with *IEC* standard, when considering REWS method, the use of remote sensing technology such as LiDAR is recommended in addition to the mast, as stated in **Section 3.6.2**, in order to determine wind speeds at various heights since LiDAR wind speed measurements correlate excellently with wind speed measurements using anemometers in meteorological masts. In this research, the power law profile was used according to **Section 3.1.1** to extrapolate wind speeds at different elevations in order to cover entire rotor disk area since, compared to the logarithmic profile, it showed to have a better model performance as indicated in **Section 5**. In addition, no remote sensing device was available and wind veer was not considered when predicting the power using REWS method.

Due to some limitations described above, some aspects listed below should be evaluated so that a comprehensive analysis can be conducted.

1. Given the large distribution of vertical wind profile types and their general transient character, relationships between those models should be investigated. In particular, the use of new method for improving the vertical extrapolation of near-surface offshore wind speeds using a machine-learning model, as mentioned in **Section 3.3**.

2. The use of REWS method considering wind veer in **Section 3.6.3**.

3. Comparison of the estimates of available power from the REWS method with the measured power output in a wind farm for the three cases presented in this study.

References

IEC 61400-12-1 Power performance measurements of electricity producing wind turbines.

Mahoney, W. P., Parks, K., Wiener, G., Liu, Y., Myers, W. L., Sun, J., Delle Monache, L., Hopson, T., Johnson, D., and Haupt. S. E. - A Wind Power Forecasting System to Optimize Grid Integration, IEEE Transactions on Sustainable Energy, 3, 670–682, 2012.

Jong, P., Dargaville, R., Silver, J., Utembe, S., Kiperstok, A., and Torres, E. A. - Forecasting high proportions of wind energy supplying the Brazilian Northeast electricity grid, Applied Energy, 195, 538 – 555, 2017.

Hasager, C. B., Madsen, P. H., Giebel, G., Réthoré, P.-E., Hansen, 390 K. S., Badger, J., Pena Diaz, A., Volker, P., Badger, M., Karagali, I., Cutululis, N. A., Maule, P., Schepers, G., Wiggelinkhuizen, J., Cantero, E., Waldl, I., Anaya-Lara, O., Attya, A. B., Svendsen, H., Palomares, A., Palma, J., Gomes, V. C., Gottschall, J., Wolken-Möhlmann, G., Bastigkeit, I., Beck, H., Trujillo, J.-J., Barthelmie, R., Sieros, G., Chaviaropoulos, T., Vincent, P., Husson, R., and Prospathopoulos, J. - Design tool for offshore wind farm cluster planning, in: Proceedings of the EWEA Annual Event and Exhibition 2015, European Wind Energy Association (EWEA), 2015.

Bahar, H., Moorhouse, J., International energy Agency – Renewable Energy Market Update: Outlook for 2021 and 2022.

Sumner, J. and Masson, C.- Influence of Atmospheric Stability on Wind Turbine Power Performance Curves, J. Sol. Energ.-T. ASME, 128, 531–538, 2006.

Wagner R, Antoniou I, Pedersen SM, Courtney MS, Jørgensen HE. The influence of the wind speed profile on wind turbine performance measurements. Wind Energy; 12: 348–362. DOI: 10.1002/we.297, 2009.

Wharton S, Lundquist JK. Atmospheric stability affects wind turbine power collection. Environmental Research Letters; 7: 014005. DOI: 10.1088/1748-9326/7/1/014005, 2012.

THOMSEN, K. - Offshore wind: a comprehensive guide to successful offshore wind farm installation, Academic Press, 2014.

HASSAN, G. G. - A guide to UK offshore wind operations and maintenance. Scottish Enterprise and The Crown Estate, 21, 2013.

Dedecca, J., Hakvoort R., Ortt, J. - Market strategies for offshore wind in Europe: A development and diffusion perspective – Renewable and Sustainable Energy Reviews, 2016.

Lumbreras S, Ramos A. - Offshore wind farm electrical design: a review. Wind Energy; 16:459–73, 2013.

Yaramasu V, Wu B, Sen PC, Kouro S, Narimani M. - High-power wind energy conversion systems: State-of-the-art and emerging technologies. Proc IEEE; 103:740–88, 2015.

Asgarpour, M. - Assembly, Transportation, Installation and Commissioning of Offshore Wind Farms. In Offshore Wind Farms, 527–41, 2016.

Paterson, J., F. D'Amico, P. R. Thies, R. E. Kurt, and G. Harrison. - "Offshore Wind Installation Vessels – A Comparative Assessment for UK Offshore Rounds 1 and 2." Ocean Engineering 148: 637–49, 2018.

Dinwoodie et al., "Reference Cases for Verification of Operation and Maintenance Simulation Models for Offshore Wind Farms," Wind engineering, 39(1), p. 1-14, 2015.

Welstead J, Hirst R, Keogh D, Robb G, Bainsfair R. - Scottish Natural Heritage Commissioned Report No. 591. Research and guidance on restoration and decommissioning of onshore wind farms, 2013.

Bradley S. - End of life opportunities. Energy Technology Institute; 2014.

Yanguas Minambres O. - Assessment of current offshore wind support structures concepts: challenges and technological requirements by 2020. Karlshochschule International University; 2012.

Ortegon K, Nies LF, Sutherland JW. - Preparing for end of service life of wind turbines. J Clean Prod; 39:191–9, 2013.

Hou, P., – Offshore Wind farm repowering. Applied Energy, 2017.

Goyal M. - Repowering-next big thing in India. Renew Sustain Energy; 14:1400–9, Rev 2010.

Hagen, B., Simonsen, I., Hofmann, M. and Muskelus, M. - "A multivariate markov weather model for O&M simulation of offshore wind parks", Energy Procedia, Vol. 35, pp. 137-147, 2013.
Shafiee, M. - "Maintenance logistics organization for offshore wind energy: current progress and future perspectives", Renewable Energy, Vol. 77, pp. 182-193, 2015a.

Breton, S.P. and Moe, G.- "Status, plans and technologies for offshore wind turbines in Europe and North America", Renewable Energy, Vol. 34 No. 3, pp. 646-654, 2009.

Utne, B.I.- "Maintenance strategies for deep-sea offshore wind turbines", Journal of Quality in Maintenance Engineering, Vol. 16 No. 4, pp. 367-381, 2010.

Victoria Baagøe-Engels Jan Stentoft - "Operations and maintenance issues in the offshore wind energy sector", International Journal of Energy Sector Management, Vol. 10 Iss 2 pp. 245 – 265, 2016.

Obhrai, C., Kalvig, S., Gudmestad Tobias, O. - A review of current guidelines and research on wind modelling for the design of offshore wind turbines, 2012.

Peterson, E. W. and Hennessey, J. P. - On the Use of Power Laws for Estimates of Wind Power Potential, J. Appl. Meteorol., 17, 390–394, 1978.

Vanderwende, B. J. and Lundquist, J. K. - The modification of wind turbine performance by statistically distinct atmospheric regimes, Environ. Res. Lett., 7, 034035, 2012.

Emeis, S. - Wind Energy Meteorology: Atmospheric Physics for Wind Power Generation, 2013.

Stull, Roland B. - Anœ Introduction to Boundary Layer Meteorology. Kluwer Academic Publ., 1988a.
——. "Similarity Theory." In An Introduction to Boundary Layer Meteorology, 347–404, 1988b.

Optis, M., Monahan, A., and Bosveld, F. C.: Moving Beyond Monin–Obukhov Similarity Theory in Modelling Wind-Speed Profiles in the Lower Atmospheric Boundary Layer under Stable Stratification, Boundary-Layer Meteorology, 153, 497–514, 2014.

Optis, M. and Monahan, A.: The Extrapolation of Near-SurfaceWind Speeds under Stable Stratification Using an Equilibrium-Based Single-Column Model Approach, Journal of Applied Meteorology and Climatology, 55, 923–943, 2016.

Panofsky, Hans A., and John A. Dutton - Atmospheric Turbulence: Models and Methods for Engineering Applications. Wiley-Interscience., 1984.

Roy, S. B., & Sharp, J. - Why Atmospheric Stability Matters in Wind Assessment, 2013.

Neumann, T., Stefan Emeis, and C. Illig. - "Report on the Research Project OWID – Offshore Wind Design Parameter." In Wind Energy, 81–85, 2007.

Tambke, Jens, Matthias Lange, Ulrich Focken, Jørg-Olaf Wolff, and John A. T. Bye. - "Forecasting Offshore Wind Speeds above the North Sea." Wind Energy 8 (1): 3–16, 2004.

Motta, M., R. J. Barthelmie, and P. Vølund. - "The Influence of Non-Logarithmic Wind Speed Profiles on Potential Power Output at Danish Offshore Sites." Wind Energy 8 (2): 219–36, 2005.

Obhrai, Charlotte, Siri Kalvig, Ove Tobias Gudmestad, and Others. - "A Review of Current Guidelines and Research on Wind Modelling for the Design of Offshore Wind Turbines." International Society of Offshore and Polar Engineers, 2012.

Eliassen, Lene, Jasna B. Jakobsen, Charlotte Obhrai, and Others. - "The Effect of Atmospheric Stability on the Fatigue Life of Offshore Wind Turbines." International Society of Offshore and Polar Engineers, 2012.

David, Afolarinwa O. - "Wind Profile Usage in Wind Farm Installation Campaign Simulations" Master thesis. Faculty of Science and Technology - University of Stavanger, 2019.

Optis, M., Bodini, N., Debnath, M. and Doubrawa, P. - New methods to improve the vertical extrapolation of near-surface offshore wind speeds, Wind Energy Science, 2021.

Bodini, N. and Optis, M. - How accurate is a machine learning-based wind speed extrapolation under a round-robin approach?, Journal of Physics: Conference Series, 1618, 062 037, IOP Publishing, 2020a.

Bodini, N. and Optis, M. - The importance of round-robin validation when assessing machine-learning-based vertical extrapolation of wind speeds, Wind Energy Science, 5, 489–501, Copernicus GmbH, 2020b.

Optis, M. and Perr-Sauer, J. - The importance of atmospheric turbulence and stability in machine-learning models of wind farm power production, Renewable and Sustainable Energy Reviews, 112, 27–41, 2019.

NORSOK N-003:2017 Actions and action effects

Holton, J. R. - An introduction to dynamic meteorology, 3rd ed., Academic Press, San Diego, 1992.

Elliott, D. L. and Cadogan, J. B. - Effects of wind shear and turbulence on wind turbine power curves, Pacific Northwest Lab., Richland, WA (USA), 1990.

Albers, A., Jakobi, T., Rohden, R., and Stoltenjohannes, J. - Influence of meteorological variables on measured wind turbine power curves, European Wind Energy Conference and Exhibition 2007, EWEC 2007, Milan, Italy, 7–10 May 3, 2007.

Walter, K., Weiss, C. C., Swift, A. H., Chapman, J., and Kelley, N. D. - Speed and Direction Shear in the Stable Nocturnal Boundary Layer, J. Sol. Energ.-T. ASME, 131, 011013-011013–7, 2009.

Murphy P, Lundquist J., Fleming Paul. - How wind speed shear and directional veer affect the power production of a megawatt-scale operational wind turbine. Wind Energ. Sci., 5, 1169–1190, 2020.

MacKay, K. P. - Steady state hodographs in a baroclinic boundary layer, Bound. -Lay. Meteorol., 2, 161–168, 1971.

Wagner, R., Courtney, M., Larsen, T. J., and Schmidt Paulsen, U. - Simulation of shear and turbulence impact on wind turbine performance, Report, Danmarks Tekniske Universitet, Risø Nationallaboratoriet for Bæredygtig Energi, Roskilde, 2010.

Sanchez Gomez, M. and Lundquist, J. K. - The effect of wind direction shear on turbine performance in a wind farm in central Iowa,Wind Energ. Sci., 5, 125–139, 2020.

Choukulkar, A., Pichugina, Y., et al. - A new formulation for rotor equivalent wind speed for wind resource assessment and wind power forecasting. Wind Energy, 2015.

Wagner R, Cañadillas B, Clifton A, et al. - Rotor equivalent wind speed for power curve measurement—comparative exercise for IEA wind annex 32, 2014.

Wächter M, Gottschall J, Rettenmeier A, Peinke J. - Power curve estimation using lidar measurements. In: Proceedings of the EWEA European Wind Energy Conference: 4473–4477; 2009.

Dupont E, Lefranc Y, Soutlier L, Koulibaly D. - Detailed analysis of uncertainty reduction on power curve determination using lidar measurements. In: Proceedings of EWEA, 2012.

Antoniou I, Pedersen SM, Enevoldsen PB. - Wind shear and uncertainties in power curve measurement and wind resources. Wind Engineering, 33: 449–468. DOI: 10.1260/030952409790291208: 2009.

Westerhellweg, A., Canadillas, B., & Neumann, T. - Direction Dependency of Offshore Turbulence Intensity in The German Bight, 2010.

Bardal LM, Sætran LR, Wangsness E. Performance test of a 3MW wind turbine—effects of shear and turbulence. Energy Procedia; 80:83-91, 2015.

Rohatgi, J. and Barbezier, G.: Wind turbulence and atmospheric stability – Their effect on wind turbine output, Renew. Energ., 16, 908–911, 1999.

Pedersen, T. F. - On wind turbine power performance measurements at inclined airflow, Wind Energy, 7, 163–176, 2004.

Van den Berg, G. P. - Wind turbine power and sound in relation to atmospheric stability, Wind Energy, 11, 151–169, 2008.

Belu, R. and Koracin, D.- Effects of complex wind regimes and meteorological parameters on wind turbine performances, IEEE Energytech, Cleveland, Ohio, 29–31 May 2012, 1–6, 2012.

Vahidzadeh, M. and Markfort, C. D. - Modified Power Curves for Prediction of Power Output of Wind Farms, Energies, 12, 1805, 2019.

Wilfried G. J. H. M. Van Sark, Van der Velde, H. C., Coelingh, J. P., and Bierbooms, W. A. A. M. - Do we really need rotor equivalent wind speed?, Wind Energy, 22, 745–763, 2019.

Beeken, A., & Kindler, D. - Technical and Environmental Research Platforms for the Benefit of the Offshore Industry. Paper presented at the BALTEXPO, Gdansk, 2011.

Westerhellweg, A., Neumann, T., & Riedel, V. - FINO1 Mast Correction. DEWI Magazin, 2012.

Kettle, A. J.: FINO 1 - Research Platform in the North Sea, 2013.

Ackerman, D. S. - Sea and Land Breezes. In., 1995.

Holtslag, M. C., W. A. A. M. Bierbooms, and G. J. W. van Bussel. - "Validation of Surface Layer Similarity Theory to Describe Far Offshore Marine Conditions in the Dutch North Sea in Scope of Wind Energy Research." Journal of Wind Engineering and Industrial Aerodynamics 136 (January): 180–91, 2015.

Øistad, Ingunn - Site analysis of the Titran Met-masts. Norwegian University of Science and Technology (NTNU), 2014.

T. Heggem. - Measurements of Coastal Wind and Temperature, Trondheim: Norwegian University of Science and Technology, 1997.

Bak, C., Zahle, F., Bitsche, R., Kim, T., Yde, A., Henriksen, L. C., Hansen, M. H., Blasques, J. P. A. A., Gaunaa, M., & Natarajan, A. - The DTU 10-MW Reference Wind Turbine. Sound/Visual production (digital), 2013.

Frank Scheurich. - Improving the Accuracy of Wind Turbine Power Curve Validation by the rotor Equivalent Wind Speed Concept. Conference Series 753: 072029. IOP Publishing - doi:10.1088/1742-6596/753/7/072029;2016.

St. Pe, A., Sperling, M., F. Brodie, J., Delgado, R. - Classifying rotor-layer wind to reduce offshore available power uncertainty - Wind Energy. DOI: 10.1002/we.2159; 2017.

Putri, R. M. - A Study of the Coherences of Turbulent Wind on a Floating Offshore Wind Turbine. University of Stavanger, Norway, 2016.

Thompson, N. - Boundary layer climates. By T. R. Oke. Methuen Ltd. 1978. Quarterly Journal of the Royal Meteorological Society, 105(446), 1084-1085. doi:10.1002/qj.49710544628, 1979.

Westerhellweg A Canadillas B, Beeken A, Neumann T. - One year of lidar measurements at FINO1-platform: comparison and verification to met‑mast data. In: Proceedings of the 10th German Wind Energy Conference DEWEK. 2010:1–5.

Ernst, B., & Seume, J. R.- Investigation of Site-Specific Wind Field Parameters and Their Effect on Loads of Offshore Wind Turbines. Energies, 5(10), 3835; 2012.

Bundesamt für Seeschifffahrt und Hydrographie. - FINO database, 2018.

Clifton A, Kilcher L, Lundquist J, Fleming P. - Using machine learning to predict wind turbine power output. Environmental Research Letters; 8: 024009. DOI: 10.1088/1748-9326/8/2/024009, 2013.

Paulsen US, Wagner R. IMPER: Characterization of the wind field over a large wind turbine rotor—final report. ISSN 0106-2840, ISBN 978-87-92896-00-1. Roskilde, Denmark: DTU. 2012.

Clack, C. T. M., Alexander, A., Choukulkar, A., and MacDonald, A. E.: Demonstrating the effect of vertical and directional shear for resource mapping of wind power, Wind Energy, 19, 1687–1697, 2016.